

# International Journal on

# Advances in Telecommunications



2009 vol. 2 nr. 4

The *International Journal on Advances in Telecommunications* is published by IARIA.

ISSN: 1942-2601

journals site: <http://www.ariajournals.org>

contact: [petre@aria.org](mailto:petre@aria.org)

Responsibility for the contents rests upon the authors and not upon IARIA, nor on IARIA volunteers, staff, or contractors.

IARIA is the owner of the publication and of editorial aspects. IARIA reserves the right to update the content for quality improvements.

Abstracting is permitted with credit to the source. Libraries are permitted to photocopy or print, providing the reference is mentioned and that the resulting material is made available at no cost.

Reference should mention:

*International Journal on Advances in Telecommunications, issn 1942-2601*  
*vol. 2, no. 4, year 2009, <http://www.ariajournals.org/telecommunications/>*

The copyright for each included paper belongs to the authors. Republishing of same material, by authors or persons or organizations, is not allowed. Reprint rights can be granted by IARIA or by the authors, and must include proper reference.

Reference to an article in the journal is as follows:

<Author list>, "<Article title>"  
*International Journal on Advances in Telecommunications, issn 1942-2601*  
*vol. 2, no. 4, year 2009,<start page>:<end page> , <http://www.ariajournals.org/telecommunications/>*

IARIA journals are made available for free, providing the appropriate references are made when their content is used.

Sponsored by IARIA

[www.aria.org](http://www.aria.org)

Copyright © 2009 IARIA

**Editor-in-Chief**

Tulin Atmaca, IT/Telecom&Management SudParis, France

**Editorial Advisory Board**

- Michael D. Logothetis, University of Patras, Greece
- Jose Neuman De Souza, Federal University of Ceara, Brazil
- Eugen Borcoci, University "Politehnica" of Bucharest (UPB), Romania
- Reijo Savola, VTT, Finland
- Haibin Liu, Aerospace Engineering Consultation Center-Beijing, China

**Advanced Telecommunications**

- Tulin Atmaca, IT/Telecom&Management SudParis, France
- Rui L.A. Aguiar, Universidade de Aveiro, Portugal
- Eugen Borcoci, University "Politehnica" of Bucharest (UPB), Romania
- Symeon Chatzinotas, University of Surrey, UK
- Denis Collange, Orange-ftgroup, France
- Todor Cooklev, Indiana-Purdue University - Fort Wayne, USA
- Jose Neuman De Souza, Federal University of Ceara, Brazil
- Sorin Georgescu, Ericsson Research, Canada
- Paul J. Geraci, Technology Survey Group, USA
- Christos Grecos, University of Central Lancashire-Preston, UK
- Manish Jain, Microsoft Research – Redmond
- Michael D. Logothetis, University of Patras, Greece
- Natarajan Meghanathan, Jackson State University, USA
- Masaya Okada, ATR Knowledge Science Laboratories - Kyoto, Japan
- Jacques Palicot, SUPELEC- Rennes, France
- Gerard Parr, University of Ulster in Northern Ireland, UK
- Maciej Piechowiak, Kazimierz Wielki University - Bydgoszcz, Poland
- Dusan Radovic, TES Electronic Solutions - Stuttgart, Germany
- Matthew Roughan, University of Adelaide, Australia
- Sergei Semenov, Nokia Corporation, Finland
- Carlos Becker Westphal, Federal University of Santa Catarina, Brazil
- Rong Zhao, Detecon International GmbH - Bonn, Germany
- Piotr Zwierzykowski, Poznan University of Technology, Poland

**Digital Telecommunications**

- Bilal Al Momani, Cisco Systems, Ireland
- Tulin Atmaca, IT/Telecom&Management SudParis, France
- Claus Bauer, Dolby Systems, USA
- Claude Chaudet, ENST, France
- Gerard Damm, Alcatel-Lucent, France
- Michael Grottke, Universitat Erlangen-Nurnberg, Germany
- Yuri Ivanov, Movidia Ltd. – Dublin, Ireland
- Ousmane Kone, UPPA - University of Bordeaux, France
- Wen-hsing Lai, National Kaohsiung First University of Science and Technology, Taiwan
- Pascal Lorenz, University of Haute Alsace, France
- Jan Lucenius, Helsinki University of Technology, Finland
- Dario Maggiorini, University of Milano, Italy
- Pubudu Pathirana, Deakin University, Australia
- Mei-Ling Shyu, University of Miami, USA

#### **Communication Theory, QoS and Reliability**

- Eugen Borcoci, University "Politehnica" of Bucharest (UPB), Romania
- Piotr Cholda, AGH University of Science and Technology - Krakow, Poland
- Michel Diaz, LAAS, France
- Ivan Gojmerac, Telecommunications Research Center Vienna (FTW), Austria
- Patrick Gratz, University of Luxembourg, Luxembourg
- Axel Kupper, Ludwig Maximilians University Munich, Germany
- Michael Menth, University of Wuerzburg, Germany
- Gianluca Reali, University of Perugia, Italy
- Joel Rodrigues, University of Beira Interior, Portugal
- Zary Segall, University of Maryland, USA

#### **Wireless and Mobile Communications**

- Tommi Aihkialo, VTT Technical Research Center of Finland - Oulu, Finland
- Zhiquan Bai, Shandong University - Jinan, P. R. China
- David Boyle, University of Limerick, Ireland
- Bezalel Gavish, Southern Methodist University - Dallas, USA
- Xiang Gui, Massey University-Palmerston North, New Zealand
- David Lozano, Telefonica Investigacion y Desarrollo (R&D), Spain
- D. Manivannan (Mani), University of Kentucky - Lexington, USA
- Himanshukumar Soni, G H Patel College of Engineering & Technology, India
- Radu Stoleru, Texas A&M University, USA
- Jose Villalon, University of Castilla La Mancha, Spain
- Natalija Vlajic, York University, Canada
- Xinbing Wang, Shanghai Jiaotong University, China
- Ossama Younis, Telcordia Technologies, USA

### **Systems and Network Communications**

- Fernando Boronat, Integrated Management Coastal Research Institute, Spain
- Anne-Marie Bosneag, Ericsson Ireland Research Centre, Ireland
- Huaqun Guo, Institute for Infocomm Research, A\*STAR, Singapore
- Jong-Hyook Lee, Sungkyunkwan University, Korea
- Elizabeth I. Leonard, Naval Research Laboratory – Washington DC, USA
- Sjouke Mauw, University of Luxembourg, Luxembourg
- Reijo Savola, VTT, Finland

### **Multimedia**

- Dumitru Dan Burdescu, University of Craiova, Romania
- Noel Crespi, Institut TELECOM SudParis-Evry, France
- Mislav Grgic, University of Zagreb, Croatia
- Christos Grecos, University of Central Lancashire, UK
- Atsushi Koike, KDDI R&D Labs, Japan
- Polychronis Koutsakis, McMaster University, Canada
- Chung-Sheng Li, IBM Thomas J. Watson Research Center, USA
- Artur R. Lugmayr, Tampere University of Technology, Finland
- Parag S. Mogre, Technische Universitat Darmstadt, Germany
- Chong Wah Ngo, University of Hong Kong, Hong Kong
- Justin Zhan, Carnegie Mellon University, USA
- Yu Zheng, Microsoft Research Asia - Beijing, China

### **Space Communications**

- Emmanuel Chaput, IRIT-CNRS, France
- Alban Duverdier, CNES (French Space Agency) Paris, France
- Istvan Frigyes, Budapest University of Technology and Economics, Hungary
- Michael Hadjitheodosiou ITT AES & University of Maryland, USA
- Mark A Johnson, The Aerospace Corporation, USA
- Massimiliano Laddomada, Texas A&M University-Texarkana, USA
- Haibin Liu, Aerospace Engineering Consultation Center-Beijing, China
- Elena-Simona Lohan, Tampere University of Technology, Finland
- Gerard Parr, University of Ulster-Coleraine, UK
- Cathryn Peoples, University of Ulster-Coleraine, UK
- Michael Sauer, Corning Incorporated/Corning R&D division, USA

**CONTENTS**

- First and Second Order Statistical Characteristics of the SSC Combiner Output Signal in the Presence of Rice fading** **111 - 120**  
Dragana Krstić, University of Niš, Serbia  
Mihajlo Stefanović, University of Niš, Serbia  
Časlav Stefanović, University of Niš, Serbia  
Petar Nikolić, Tigartyres, Serbia  
Zoran Popović, University of Kragujevac, Serbia
- Dynamic Power and Bit Allocation Scheme for Spectral Efficiency Maximization in Cognitive Multiband OFDM UWB Systems** **121 - 130**  
Liaoyuan Zeng, University of Limerick, Ireland  
Sean McGrath, University of Limerick, Ireland  
Eduardo Cano, Institute for the Protection and Security of the Citizen Joint Research Center European Commission, Italy
- Adaptive MCS Selection with Dynamic and Fixed Sub-channelling for Frequency-Coherent OFDM Channels** **131 - 141**  
Muayad S. Al-Janabi, Newcastle University, UK  
Charalampos C. Tsimenidis, Newcastle University, UK  
Bayan S. Sharif, Newcastle University, UK  
Stéphane Y. Le Goff, Newcastle University, UK

## First and Second Order Statistical Characteristics of the SSC Combiner Output Signal in the Presence of Rice fading

Dragana Krstić, Mihajlo Stefanović  
Faculty of Electronic Engineering  
University of Niš  
Aleksandra Medvedeva 14,  
18000 Niš, Serbia  
dragana.krstic@elfak.ni.ac.rs

Časlav Stefanović  
Faculty of Electronic Engineering  
University of Niš  
Aleksandra Medvedeva 14,  
Niš, Serbia  
caslav.stefanovic@gmail.com

Petar Nikolić  
Tigartyres, Pirot  
Nikole Pašica 99,  
18300 Pirot, Serbia  
p.nikolic@tigartyres.com

Zoran Popović  
Technical Faculty of Čačak  
University of Kragujevac  
Svetog Save 65,  
32000 Čačak, Serbia  
pop@tfc.kg.ac.rs

**Abstract**— The level crossing rate, the outage probability, the average time of fade duration and the bit error rate of the Switch and Stay Combiner (SSC) output signal, in the presence of Rice fading at the input, are determined in this paper. The results are shown graphically for different variance values, decision threshold values and signal and fading parameters values.

**Keywords**- probability density function, level crossing rate, outage probability, average fade duration, bit error rate, Switch and Stay Combiner, Rice fading

### I. INTRODUCTION

The most important obstruction in wireless telecommunication systems is fading. When a received signal experiences fading during transmission, its envelope and phase both fluctuate over time. The fading appears because of signals extending by more paths and shadow effects. Last few years, with development of wireless and mobile communication systems, this problem is considered in the literature [2], [3].

Many of the wireless communication systems use some form of diversity combining in order to reduce multipath fading appeared in the channel. Upgrading transmission reliability and increasing channel capacity without increasing transmission power and bandwidth is the main goal of diversity techniques.

The most useful are space diversity with two or more branches. The receiver combines signals from different antenna and makes the decision from combined signal on the optimal manner. The most popular of them are maximal ratio combining (MRC), equal gain combining (EGC), selection combining (SC) and switch and stay combining (SSC).

Maximal-Ratio Combining (MRC) is one of the most widely used diversity combining schemes whose SNR is the sum of the SNR's of each individual diversity branches. MRC is the optimal combining scheme, but its price and

complexity are higher. Also, MRC requires cognition of all channel parameters and admit in the same phase all input signals, because it is the most complicated for realization ([4]-[6]).

Signal at the EGC diversity system output is equal to the sum of its' input signals. The input signals should be admitted in the same phase, but it is not necessary to know the channel parameters. Therefore, EGC provides comparable performances to MRC technique, but has lower implementation complexity, so it is an intermediate solution [7].

Among the simpler diversity combining schemes, selection combining (SC) and switch and stay combining (SSC) are the two most popular. With SC receiver, the processing is performed at only one of the diversity branches, which is selectively chosen, and no channel information is required. That is why SC is much simpler for practical realization. In general, selection combining, assuming that noise power is equally distributed over branches, selects the branch with the highest signal-to-noise ratio (SNR) that is the branch with the strongest signal ([7]-[9]).

SSC is an attempt to simplify the complexity of the system with loss in performance. In this case, rather than continually connecting the antenna with the best fading conditions, the receiver selects a particular antenna until its quality drops below a predetermined threshold. When this happens, the receiver switches to another antenna and stays with it for the next time slot, regardless of whether or not the channel quality of that antenna is above or below the predetermined threshold.

The consideration of SSC systems in the literature has been restricted to low-complexity mobile units where the number of diversity antennas is typically limited to two ([10]-[12]). Furthermore, in all these publications, only

predetection SSC has thus far been considered wherein the switching of the receiver between the two receiving antennas is based on a comparison of the instantaneous signal to noise ratio (SNR) of the connected antenna with a predetermined threshold. This results in a reduction of complexity relative to SC in that the simultaneous and continuous monitoring of both branches SNRs is no longer necessary. In [13] the moment generating function (MGF) of the signal power at the output of dual-branch switch and stay selection diversity (SSC) combiners is derived.

The fading influence to the system performances is considered in [2]. The most often Rayleigh, Rice, Nakagami, Weibull and log-normal fading are considered.

The Rice fading is present very often in wireless telecommunication systems with direct line of site. When the fading appeared in the channel because of signal propagation by more paths, and dominate component exists because of optical visibility from transmitter to receiver, signal amplitude is modeled by Rice distribution. Therefore, *Rice distribution* is often used to model propagation paths consisting of one strong direct LOS component and many random weaker components.

Abu-Dayya and Beaulieu in [14] consider switched diversity on microcellular Ricean channels.

The performances of the SSC combiner output signal in the presence of Nakagami-m fading are assigned in [15] and in the presence of log-normal fading in [16]. The level crossing rate of the SSC combiner output signal in the presence of Rayleigh fading is observed in [17].

The probability density function of dual branch SSC combiner output signal and the joint probability density function of this combiner output signal at two time instants in the presence of Rice fading are settled in [18].

The level crossing rate of the SSC combiner output signal in the presence of Rice fading is calculated and presented in [19] and the outage probability and the average time of fade duration of the SSC combiner output signal in the presence of Rice fading at the input are determined in [1].

Because the switch and stay combining (SSC) is very popular combining model due to its simplicity, their performances in the presence of Rice fading are summed up in this paper. Whereas the level crossing rate, the outage probability and the average fade duration for dual SSC combiner are determined earlier, the bit error rate of the SSC combiner output signal in the presence of Rice fading for coherent BPSK modulation scheme will be determined in this paper. The results will be shown graphically for different signal and fading parameters values and the decision threshold values.

The structure of the paper is as follows: after Introduction in Section II the model of the SSC combiner is given. Then, in Section III, the system performances are derived. In Section IV the numerical results for all performances are given in the case that BPSK modulation scheme is considered. The last Section is Conclusion.

## II. SYSTEM MODEL

With SSC combiner with great number of branches we can minimize the bit error rate (BER). We will analyze in this paper the SSC combiner with two inputs because the gain is the greatest when instead of one-channel system at least the dual SSC combiner is used. With the enlarging of the number of inputs (branches) the gain becomes less. Because of that it is more economic using dual SSC combiner.

The model of the SSC combiner with two inputs, considered in this paper, is shown in Figure 1.

The signals at the combiner input are  $r_1$  and  $r_2$ , and  $r$  is the combiner output signal. The predetection combining is observed.

The probability of the event that the combiner first examines the signal at the first input is  $P_1$ , and for the second input to be examined first it is  $P_2$ .

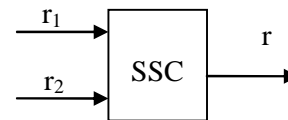


Figure 1. Model of the SSC combiner with two inputs

If the combiner examines first the signal at the first input and if the value of the signal at the first input is above the decision threshold,  $r_T$ , SSC combiner forwards this signal to the circuit for the decision. If the value of the signal at the first input is below the decision threshold  $r_T$ , SSC combiner forwards the signal from the other input to the circuit for the decision. If the SSC combiner first examines the signal from the second combiner input it works in the similar way.

The decision threshold value can be selected so that one of three parameters has to be minimal: the error probability, fade duration or average signal value (or signal to noise/interference ratio (SNR/SIR) when noise or interference is significant) [2].

The average SNR at the SSC output can be obtained by averaging  $\gamma$  over  $p_{\gamma SSC}(\gamma)$  as given by [2, Eq. 9.274], yielding

$$\begin{aligned} \bar{\gamma}_{SSC} &= p_{\gamma}(\gamma_T) \int_0^{\infty} \gamma p_{\gamma}(\gamma) d\gamma + \int_{\gamma_T}^{\infty} \gamma p_{\gamma}(\gamma) d\gamma = \\ &= p_{\gamma}(\gamma_T) \bar{\gamma} + \int_{\gamma_T}^{\infty} \gamma p_{\gamma}(\gamma) d\gamma \end{aligned}$$

Differentiating previous equation with respect to  $\gamma_T$  and setting the result to zero, it can be easily shown that  $\bar{\gamma}_{SSC}$  is maximized when the switching threshold is set to  $\gamma_T^* = \bar{\gamma}$ .

It can be shown that the MGF associated with appropriate fading model is given by [2, Eq. 2.17], and the moments are given by [2, Eq. (2.18)]

$$E(\gamma^k) = \frac{\Gamma(1+k)}{(1+n^2)^k} {}_1F_1(-k, 1; -n^2) \bar{\gamma}^k$$

where  ${}_1F_1(\cdot, \cdot; \cdot)$  is the Kummer confluent hypergeometric function and parameter  $k=1$  for the presence of Rice fading.

### III. SYSTEM PERFORMANCES

The determination of the probability density of the combiner output signal is important for the receiver performance determination.

The probability density functions (PDFs) of the combiner input signals,  $r_1$  and  $r_2$ , in the presence of Rice fading, are [20]:

$$p_{r_i}(r_i) = \frac{r_i}{\sigma_i^2} e^{-\frac{r_i^2 + A^2}{2\sigma_i^2}} I_0\left(\frac{r_i A}{\sigma_i^2}\right) \quad r_i \geq 0 \quad (1)$$

where  $i=1,2$ ;  $A$  is the signal amplitude,  $\sigma_1$  and  $\sigma_2$  are variances.

The cumulative probability densities (CDFs) are given by [2]:

$$F_{r_i}(r_T) = \int_0^{r_T} p_{r_i}(x) dx \quad (2)$$

where  $i=1,2$  and  $r_T$  is the decision threshold.

If we put the expression (1) into (2), we obtain the CDFs in the presence of Rice fading as:

$$F_{r_i}(r_T) = \int_0^{r_T} \frac{x}{\sigma_i^2} e^{-\frac{x^2 + A^2}{2\sigma_i^2}} I_0\left(\frac{x A}{\sigma_i^2}\right) dx = 1 - Q(A/\sigma_i, r_T/\sigma_i) \quad (3)$$

for  $i=1,2$ .  $Q(a,b)$  is the Marcum  $Q$  function defined as [2]:

$$Q(a, b) = \int_b^\infty t \exp\left[-\frac{t^2 + a^2}{2}\right] I_0(at) dt .$$

The joint probability densities of the combiner input signals,  $r_1$  and  $r_2$ , and their derivatives  $\dot{r}_1$  and  $\dot{r}_2$ , in the presence of Rice fading, are [3]:

$$p_{r_1 \dot{r}_1}(r_1, \dot{r}_1) = \frac{r_1}{\sigma_1^2} e^{-\frac{r_1^2 + A^2}{2\sigma_1^2}} \cdot I_0\left(\frac{r_1 A}{\sigma_1^2}\right) \cdot \frac{1}{\sqrt{2\pi} \beta_1} e^{-\frac{\dot{r}_1^2}{2\beta_1^2}}, \quad r_1 \geq 0 \quad (4)$$

$$p_{r_2 \dot{r}_2}(r_2, \dot{r}_2) = \frac{r_2}{\sigma_2^2} e^{-\frac{r_2^2 + A^2}{2\sigma_2^2}} \cdot I_0\left(\frac{r_2 A}{\sigma_2^2}\right) \cdot \frac{1}{\sqrt{2\pi} \beta_2} e^{-\frac{\dot{r}_2^2}{2\beta_2^2}}, \quad r_2 \geq 0 \quad (5)$$

where  $\beta_1$  and  $\beta_2$  are variances.

The expression for the joint probability density function of the SSC combiner output signal and its derivative will be determined first for the case  $r < r_T$ :

$$p_{r\dot{r}}(r\dot{r}) = P_1 \cdot F_{r_1}(r_T) \cdot p_{r_2 \dot{r}_2}(r\dot{r}) + P_2 \cdot F_{r_2}(r_T) \cdot p_{r_1 \dot{r}_1}(r\dot{r}) \quad (6)$$

and then for  $r \geq r_T$ :

$$p_{r\dot{r}}(r\dot{r}) = P_1 \cdot F_{r_1}(r_T) \cdot p_{r_2 \dot{r}_2}(r\dot{r}) + P_1 \cdot \dot{r}_1(r\dot{r}) + P_2 \cdot \dot{r}_2(r\dot{r}) + P_2 \cdot F_{r_2}(r_T) \cdot p_{r_1 \dot{r}_1}(r\dot{r}) \quad (7)$$

The expressions for the obtainment of the probabilities  $P_1$  and  $P_2$  are [19]:

$$P_1 = P_1(1 - F_{r_1}(r_T)) + P_2 F_{r_2}(r_T) \quad (8)$$

$$P_2 = P_2(1 - F_{r_2}(r_T)) + P_1 F_{r_1}(r_T) \quad (9)$$

Then, after arrangement, the probabilities  $P_1$  and  $P_2$  are:

$$P_1 = \frac{F_{r_2}(r_T)}{F_{r_1}(r_T) + F_{r_2}(r_T)} \quad (10)$$

$$P_2 = \frac{F_{r_1}(r_T)}{F_{r_1}(r_T) + F_{r_2}(r_T)} \quad (11)$$

After changing (3) into (10), i.e. (11), it is valid [16]:

$$P_1 = \frac{1 - Q(A/\sigma_2, r_T/\sigma_2)}{2 - [Q(A/\sigma_1, r_T/\sigma_1) + Q(A/\sigma_2, r_T/\sigma_2)]} \quad (12)$$

$$P_2 = \frac{1 - Q(A/\sigma_1, r_T/\sigma_1)}{2 - [Q(A/\sigma_1, r_T/\sigma_1) + Q(A/\sigma_2, r_T/\sigma_2)]} \quad (13)$$

The expression for the joint probability density function (pdf) of the SSC combiner output signal and its derivative, in the presence of Rice fading, after substitutions of the expressions (3), (12) and (13) into (6) for the case  $r < r_T$  is:

$$p_{r\dot{r}}(r\dot{r}) = B \cdot \frac{r}{\sigma_2^2} e^{-\frac{r^2+A^2}{2\sigma_2^2}} I_0\left(\frac{rA}{\sigma_2^2}\right) \cdot I_0\left(\frac{rA}{\sigma^2}\right) \cdot \frac{1}{\sqrt{2\pi}\beta} e^{-\frac{\dot{r}^2}{2\beta^2}} \quad (17)$$

$$\cdot \frac{1}{\sqrt{2\pi}\beta_2} e^{-\frac{\dot{r}^2}{2\beta_2^2}} + B \cdot \frac{r}{\sigma_1^2} e^{-\frac{r^2+A^2}{2\sigma_1^2}} \cdot I_0\left(\frac{rA}{\sigma_1^2}\right) \cdot \frac{1}{\sqrt{2\pi}\beta_1} e^{-\frac{\dot{r}^2}{2\beta_1^2}} \quad (14)$$

where:

$$B = \frac{(1-Q(A/\sigma_1, r_T/\sigma_1))(1-Q(A/\sigma_2, r_T/\sigma_2))}{2 - [Q(A/\sigma_1, r_T/\sigma_1) + Q(A/\sigma_2, r_T/\sigma_2)]} \quad (15)$$

For  $r \geq r_T$  the joint pdf of the SSC combiner output signal and its derivative, in the presence of Rice fading, after substitutions of the expressions (3), (12) and (13) into (7), is:

$$p_{r\dot{r}}(r\dot{r}) = \frac{1 - Q(A/\sigma_2, r_T/\sigma_2)}{2 - [Q(A/\sigma_1, r_T/\sigma_1) + Q(A/\sigma_2, r_T/\sigma_2)]} \cdot \frac{r}{\sigma_1^2} e^{-\frac{r^2+A^2}{2\sigma_1^2}} I_0\left(\frac{rA}{\sigma_1^2}\right) \cdot \frac{1}{\sqrt{2\pi}\beta_1} e^{-\frac{\dot{r}^2}{2\beta_1^2}} +$$

$$+ B \cdot \frac{r}{\sigma_2^2} e^{-\frac{r^2+A^2}{2\sigma_2^2}} I_0\left(\frac{rA}{\sigma_2^2}\right) \cdot \frac{1}{\sqrt{2\pi}\beta_2} e^{-\frac{\dot{r}^2}{2\beta_2^2}} +$$

$$+ \frac{1 - Q(A/\sigma_1, r_T/\sigma_1)}{2 - [Q(A/\sigma_1, r_T/\sigma_1) + Q(A/\sigma_2, r_T/\sigma_2)]} \cdot \frac{r}{\sigma_2^2} e^{-\frac{r^2+A^2}{2\sigma_2^2}} I_0\left(\frac{rA}{\sigma_2^2}\right) \cdot \frac{1}{\sqrt{2\pi}\beta_2} e^{-\frac{\dot{r}^2}{2\beta_2^2}} +$$

$$+ B \cdot \frac{r}{\sigma_1^2} e^{-\frac{r^2+A^2}{2\sigma_1^2}} I_0\left(\frac{rA}{\sigma_1^2}\right) \cdot \frac{1}{\sqrt{2\pi}\beta_1} e^{-\frac{\dot{r}^2}{2\beta_1^2}} \quad (16)$$

For the channels with identical parameters:  $\beta_1 = \beta_2 = \beta$  and  $\sigma_1 = \sigma_2 = \sigma$  and for  $r < r_T$  the joint probability density function of the SSC combiner output signal and its derivative is:

$$p_{r\dot{r}}(r\dot{r}) = (1 - Q(A/\sigma, r_T/\sigma)) \cdot \frac{r}{\sigma^2} e^{-\frac{r^2+A^2}{2\sigma^2}} \cdot$$

and for  $r \geq r_T$  the joint pdf is:

$$p_{r\dot{r}}(r\dot{r}) = (2 - Q(A/\sigma, r_T/\sigma)) \cdot \frac{r}{\sigma^2} e^{-\frac{r^2+A^2}{2\sigma^2}} \cdot I_0\left(\frac{rA}{\sigma^2}\right) \cdot \frac{1}{\sqrt{2\pi}\beta} e^{-\frac{\dot{r}^2}{2\beta^2}} \quad (18)$$

The level crossing rate is [2]:

$$N(r_{th}) = \int_0^\infty \dot{r} p_{r\dot{r}}(r_{th}, \dot{r}) d\dot{r} \quad (19)$$

After some calculations the expressions for the level crossing rate are obtained in [16]. These expressions for the channels with identical parameters are, for  $r_{th} < r_T$ :

$$N(r_{th}) = (1 - Q(A/\sigma, r_T/\sigma)) \cdot \frac{r_{th}}{\sigma^2} e^{-\frac{r_{th}^2+A^2}{2\sigma^2}} \cdot I_0\left(\frac{r_{th}A}{\sigma^2}\right) \frac{\beta}{\sqrt{2\pi}} \quad (20)$$

and for  $r_{th} \geq r_T$ :

$$N(r_{th}) = (2 - Q(A/\sigma, r_T/\sigma)) \cdot \frac{r_{th}}{\sigma^2} e^{-\frac{r_{th}^2+A^2}{2\sigma^2}} \cdot I_0\left(\frac{r_{th}A}{\sigma^2}\right) \frac{\beta}{\sqrt{2\pi}} \quad (21)$$

The probability density function is used for the system error probability and for the outage probability determination. The probability density functions of the output signal is, for  $r < r_T$ :

$$p_r(r) = P_1 \cdot F_{r_1}(r_T) \cdot p_{r_2}(r) + P_2 \cdot F_{r_2}(r_T) \cdot p_{r_1}(r) \quad (22)$$

and for  $r \geq r_T$  the pdf is:

$$p_r(r) = P_1 \cdot p_{r_1}(r) + P_1 \cdot F_{r_1}(r_T) \cdot p_{r_2}(r) + P_2 \cdot p_{r_2}(r) + P_2 \cdot F_{r_2}(r_T) \cdot p_{r_1}(r) \quad (23)$$

After some substitutions of the expressions (3), (12) and (13) into (22), i.e. (23), the pdf, for  $r < r_T$ , is:

$$p_r(r) = B \cdot \frac{r}{\sigma_2^2} e^{-\frac{r^2+A^2}{2\sigma_2^2}} I_0\left(\frac{rA}{\sigma_2^2}\right) + B \cdot \frac{r}{\sigma_1^2} e^{-\frac{r^2+A^2}{2\sigma_1^2}} I_0\left(\frac{rA}{\sigma_1^2}\right) \quad (24)$$

where  $B$  is defined in (15).

For  $r \geq r_T$  the pdf is:

$$p_r(r) = P_1 \cdot \frac{r}{\sigma_1^2} e^{-\frac{r^2+A^2}{2\sigma_1^2}} I_0\left(\frac{rA}{\sigma_1^2}\right) + B \cdot \frac{r}{\sigma_2^2} e^{-\frac{r^2+A^2}{2\sigma_2^2}} I_0\left(\frac{rA}{\sigma_2^2}\right) + P_2 \cdot \frac{r}{\sigma_2^2} e^{-\frac{r^2+A^2}{2\sigma_2^2}} I_0\left(\frac{rA}{\sigma_2^2}\right) + B \cdot \frac{r}{\sigma_1^2} e^{-\frac{r^2+A^2}{2\sigma_1^2}} \cdot I_0\left(\frac{rA}{\sigma_1^2}\right) \quad (25)$$

$P_1$  and  $P_2$  are given by (12) and (13).

The outage probability  $P_{out}$  is standard performance criterion of communication systems operating over fading channels. This performance measure is commonly used to control the noise or co-channel interference level, helping the designers of wireless communication systems to meet the quality-of-service (QoS) and grade of service (GoS) demands.

The outage probability  $P_{out}$  is defined as the probability that the combiner output SNR falls below a given threshold  $\gamma_{th}$  and is therefore obtained by replacing  $\gamma$  with  $\gamma_{th}$  in the CDF expressions given previously.

The outage probability  $P_{out}(r_{th})$  is defined as [2]:

$$P_{out}(r_{th}) = \int_0^{r_{th}} p_r(r) dr \quad (26)$$

After appropriate substitutions the outage probabilities are, for  $r_{th} < r_T$  [1]:

$$P_{out}(r_{th}) = B \cdot (1 - Q(A/\sigma_1, r_{th}/\sigma_1)) + B \cdot (1 - Q(A/\sigma_2, r_{th}/\sigma_2)) \quad (27)$$

and for  $r_{th} \geq r_T$ :

$$P_{out}(r_{th}) = P_1 \cdot (Q(A/\sigma_1, r_T/\sigma_1) - Q(A/\sigma_1, r_{th}/\sigma_1)) +$$

$$+ B \cdot (1 - Q(A/\sigma_1, r_{th}/\sigma_1)) + P_2 \cdot (Q(A/\sigma_2, r_T/\sigma_2) - Q(A/\sigma_2, r_{th}/\sigma_2)) + B \cdot (1 - Q(A/\sigma_2, r_{th}/\sigma_2)) + \quad (28)$$

For the channels with identical parameters it is valid, for  $r_{th} < r_T$ :

$$P_{out}(r_{th}) = (1 - Q(A/\sigma, r_T/\sigma))(1 - Q(A/\sigma, r_{th}/\sigma)) \quad (29)$$

and for  $r_{th} \geq r_T$ :

$$P_{out}(r_{th}) = (1 - Q(A/\sigma, r_T/\sigma))(1 - Q(A/\sigma, r_{th}/\sigma)) + Q(A/\sigma_1, r_T/\sigma_1) - Q(A/\sigma_1, r_{th}/\sigma_1) \quad (30)$$

The average time of fade duration can be obtained from the expression [2]:

$$T(r_{th}) = \frac{P_{out}(r_{th})}{N(r_{th})} \quad (31)$$

Substituting (20) and (27) in (31), the average fade duration  $T(r_{th})$  can be obtained for  $r_{th} < r_T$  as:

$$T(r_{th}) = \frac{B \cdot (1 - Q(A/\sigma_1, r_{th}/\sigma_1)) + B \cdot (1 - Q(A/\sigma_2, r_{th}/\sigma_2))}{(1 - Q(A/\sigma, r_T/\sigma)) \frac{r_{th}}{\sigma^2} e^{-\frac{r_{th}^2+A^2}{2\sigma^2}} \cdot I_0\left(\frac{r_{th}A}{\sigma^2}\right) \frac{\beta}{\sqrt{2\pi}}} \quad (32)$$

Substituting (21) and (28) in (31), the average fade duration  $T(r_{th})$  is, for  $r_{th} \geq r_T$ :

$$T(r_{th}) = \frac{1}{(2 - Q(A/\sigma, r_T/\sigma)) \frac{r_{th}}{\sigma^2} e^{-\frac{r_{th}^2+A^2}{2\sigma^2}} \cdot I_0\left(\frac{r_{th}A}{\sigma^2}\right) \frac{\beta}{\sqrt{2\pi}}} \cdot (P_1 \cdot (Q(A/\sigma_1, r_T/\sigma_1) - Q(A/\sigma_1, r_{th}/\sigma_1)) + B \cdot (1 - Q(A/\sigma_1, r_{th}/\sigma_1)) + P_2 \cdot (Q(A/\sigma_2, r_T/\sigma_2) - Q(A/\sigma_2, r_{th}/\sigma_2)) + B \cdot (1 - Q(A/\sigma_2, r_{th}/\sigma_2))) + \quad (33)$$

The bit error rate (BER) is given by [2]:

$$P_b(e) = \int_0^{\infty} P_b(e/r) p_r(r) dr \quad (34)$$

where,  $P_b(e/r)$  is conditional BER and  $p_r(r)$  is the pdf of the combiner output signal  $r$  [2]

$$P_b(e/\gamma) = Q(\sqrt{2g\gamma}) \quad (35)$$

and  $Q$  is the one-dimensional Gaussian Q-function [2]

$$Q(x) = \frac{1}{\sqrt{2\pi}} \int_x^{\infty} e^{-t^2/2} dt \quad (36)$$

Gaussian Q-function can be defined using alternative form as [2, 21]:

$$Q(x) = \frac{1}{\pi} \int_0^{\pi/2} \exp\left(-\frac{x^2}{2\sin^2\phi}\right) d\phi \quad (37)$$

After putting (35) and (37) in (34),  $P_b(e)$  is obtained as

$$P_b(e) = \frac{1}{\pi} \int_0^{\infty} \int_0^{\pi/2} \exp\left(-\frac{gr}{\sin^2\phi}\right) p_r(r) d\phi dr. \quad (38)$$

For coherent BPSK parameter  $g$  is determined as  $g=1$  [22] and  $P_b(e)$  is given by

$$P_b(e) = \frac{1}{\pi} \int_0^{\infty} \int_0^{\pi/2} \exp\left(-\frac{r}{\sin^2\phi}\right) p_r(r) d\phi dr. \quad (39)$$

For SSC combiner output signal in the presence of Rice fading, BER is:

$$\begin{aligned} P_b(e) &= \frac{1}{\pi} \int_0^{\infty} \int_0^{\pi/2} \exp\left(-\frac{r}{\sin^2\phi}\right) \cdot \\ &\cdot \left[ B \cdot \frac{r}{\sigma_1} e^{-\frac{r^2+A^2}{2\sigma_1^2}} I_0\left(\frac{rA}{\sigma_1}\right) + \right. \\ &+ \left. B \frac{r}{\sigma_2} e^{-\frac{r^2+A^2}{2\sigma_2^2}} I_0\left(\frac{rA}{\sigma_2}\right) \right] d\phi dr + \\ &+ \frac{1}{\pi} \int_{r_T}^{\infty} \int_0^{\pi/2} \exp\left(-\frac{r}{\sin^2\phi}\right) \cdot \\ &\cdot \left[ P_1 \cdot \frac{r}{\sigma_1} e^{-\frac{r^2+A^2}{2\sigma_1^2}} I_0\left(\frac{rA}{\sigma_1}\right) + \right. \end{aligned}$$

$$\left. + P_2 \cdot \frac{r}{\sigma_2} e^{-\frac{r^2+A^2}{2\sigma_2^2}} I_0\left(\frac{rA}{\sigma_2}\right) \right] d\phi dr \quad (40)$$

#### IV. NUMERICAL RESULTS

The joint probability density functions (PDFs) of the SSC combiner output signal and its derivative  $p_{rr}(r, \dot{r})$  are shown in Figures 2. and 3.

The parameters of curves are some different values of the decision threshold  $r_T$ , variances  $\sigma$  and  $\beta$  and the signal amplitude  $A$ .

The probability density functions are used for the system error probability and for the outage probability determination.

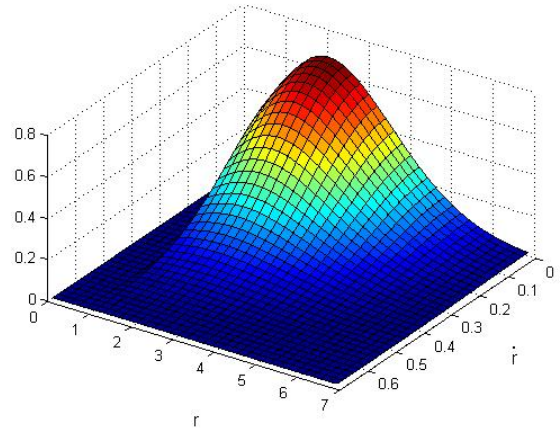


Figure 2. The joint PDF of the SSC combiner output signal and its derivative for  $r_T = 1, \sigma = 2, A = 0.5$  and  $\beta = 0.2$

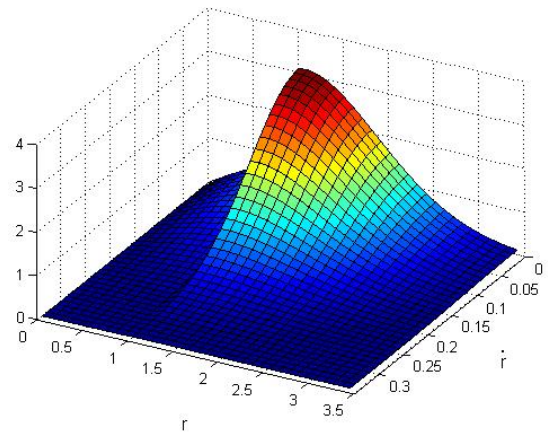


Figure 3. The joint PDF of the SSC combiner output signal and its derivative for  $r_T = 1, \sigma = 1, A = 0.5$  and  $\beta = 0.1$

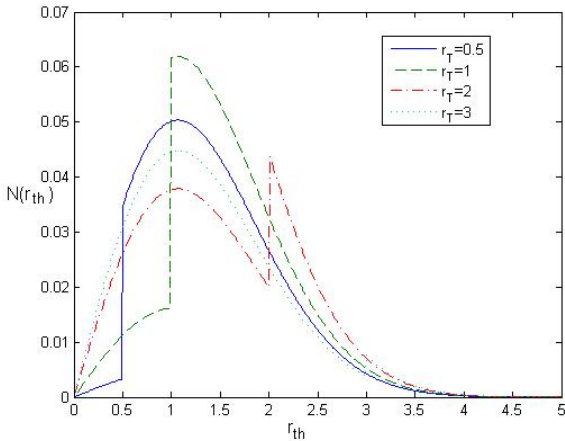


Figure 4. The level crossing rate  $N(r_{th})$  for  $r_T = 0.5; 1; 2; 3$ ,  $\sigma = 1$ ,  $A = 0.5$  and  $\beta = 0.2$

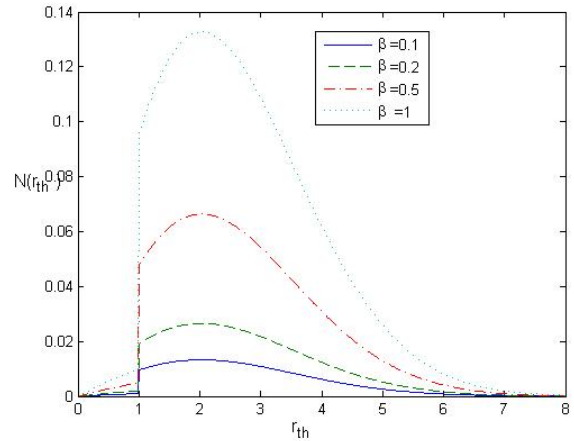


Figure 7. The level crossing rate  $N(r_{th})$  for  $r_T = 1$ ,  $\sigma = 2$ ,  $A = 0.5$  and  $\beta = 0.1; 0.2; 0.5; 1$

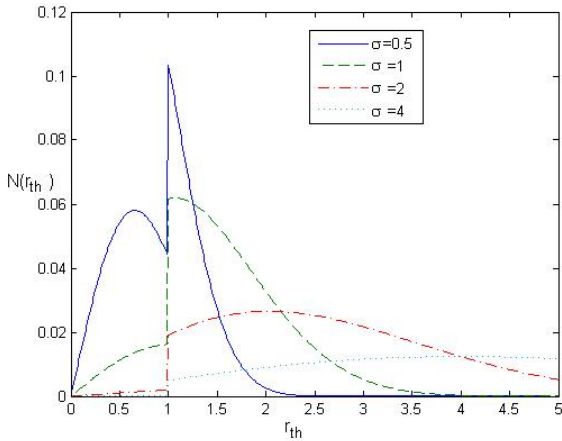


Figure 5. The level crossing rate  $N(r_{th})$  for  $r_T = 1$ ,  $\sigma = 0.5; 1; 2; 4$ ,  $A = 0.5$  and  $\beta = 0.2$

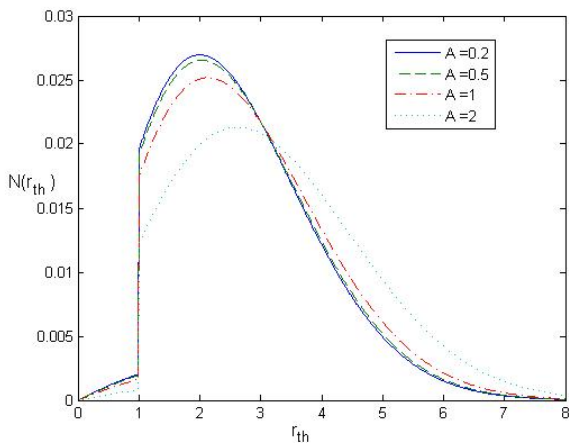


Figure 6. The level crossing rate  $N(r_{th})$  for  $r_T = 1$ ,  $\sigma = 2$ ,  $A = 0.2; 0.5; 1; 2$  and  $\beta = 0.2$

The level crossing rate curves  $N(r_{th})$  versus decision threshold value are given in Figures 4. to 7. for different values of variances  $\sigma$  and  $\beta$ , threshold value  $r_T$  and amplitude  $A$ .

We can notice from the Figures 4. to 7, that all represented curves have the same shape, but there is discontinuities on the level crossing rate curves versus threshold. Numerical values of the threshold determine the discontinuity moment appearance.

The outage probability curves,  $P_{OUT}(r_{th})$ , versus the threshold, are shown for some parameter values in Figures 8. and 9. The outage probability curves, versus the threshold, given in Figure 8, are with the parameter of curves  $r_T$ . The parameter of the curves from Figure 9. is the variance  $\sigma$ .

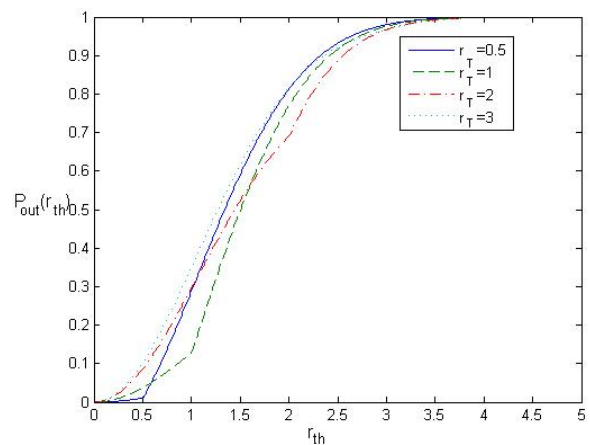


Figure 8. The outage probability  $P_{OUT}(r_{th})$  for  $r_T = 0.5; 1; 2; 3$ ,  $\sigma = 1$ ,  $A = 0.5$

From Figure 8. can be seen that the outage probability increases with rising of the threshold. The represented curves have similar shape, but there is discontinuities on them versus the threshold value. Numerical values of the threshold determine the discontinuity moment appearance.

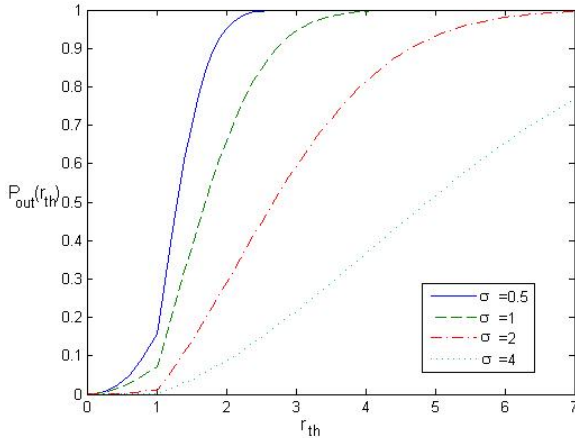


Figure 9. The outage probability  $P_{OUT}(r_{th})$  for  $r_T = 1, \sigma = 0.5; 1; 2; 4, A = 0.5$

From Figure 9. can be seen that the outage probability increases with rising of the threshold. The represented curves have similar shape, but there is also discontinuities on them versus the threshold value. The curves are steeper when variance  $\sigma$  is less.

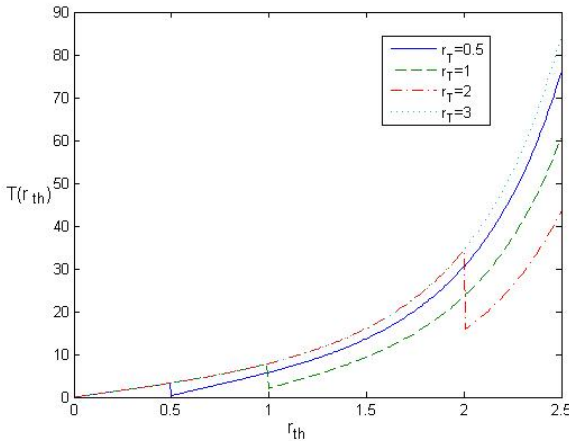


Figure 10. The fade duration  $T(r_{th})$  for  $r_T = 0.5; 1; 2; 3, \sigma = 1, A = 0.5$  and  $\beta = 0.2$

The fade duration curves,  $T(r_{th})$ , are shown in Figures 10. to 13. versus the decision threshold, for different parameter values.

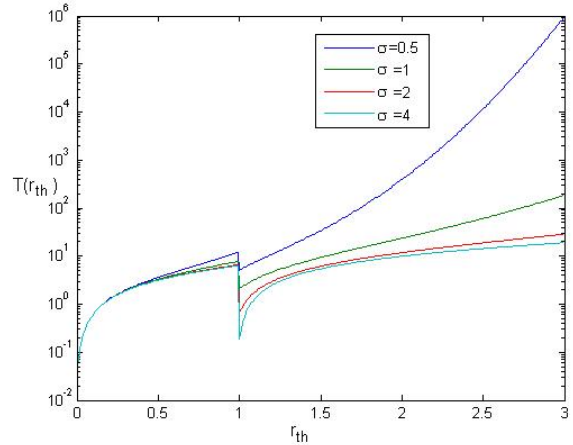


Figure 11. The fade duration  $T(r_{th})$  for  $r_T = 1, \sigma = 0.5; 1; 2; 4, A = 0.5$  and  $\beta = 0.2$

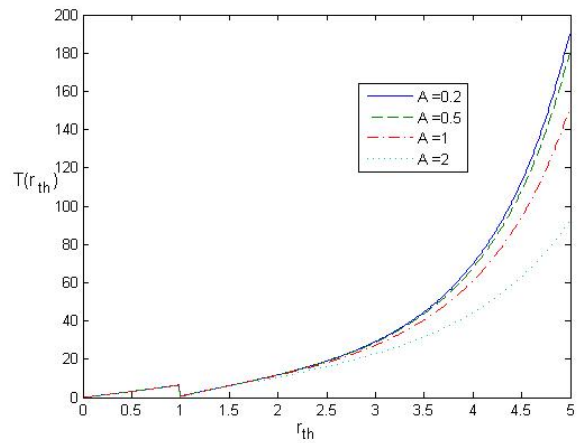


Figure 12. The fade duration  $T(r_{th})$  for  $r_T = 1, \sigma = 2, A = 0.2; 0.5; 1; 2$  and  $\beta = 0.2$

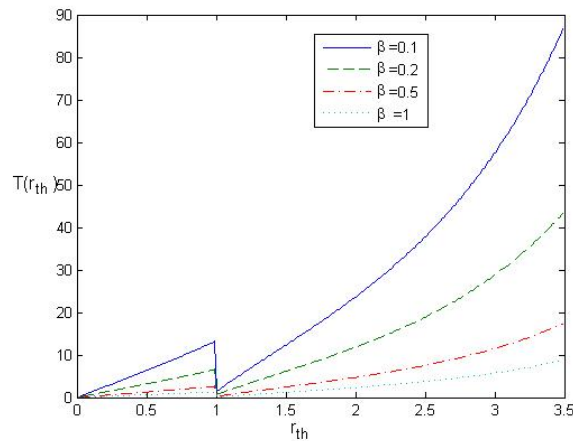


Figure 13. The fade duration  $T(r_{th})$  for  $r_T = 1, \sigma = 2, A = 0.5$  and  $\beta = 0.1; 0.2; 0.5; 1$

We can compare these figures now. It can be observed that all curves,  $T(r_{th})$  versus decision threshold, have similar shape, but threshold numerical value influence to the discontinuity moment appearance. Larger rise of fade duration corresponds to larger threshold values and to less variances  $\sigma$  and  $\beta$ , and signal amplitude  $A$ .

The bit error rate curves,  $P_b(e)$ , for different parameters, are illustrated in Figures 14. to 17.

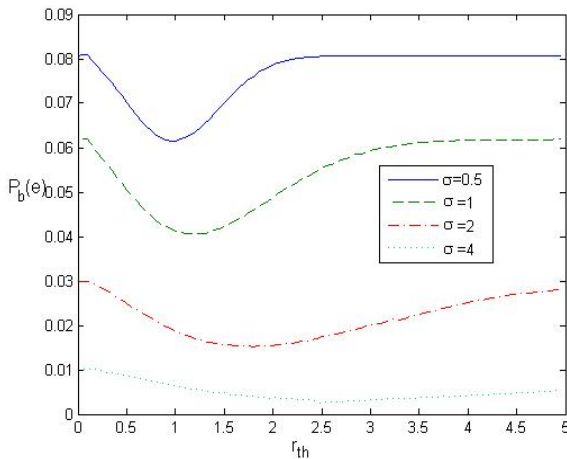


Figure 14. The bit error rate  $P_b(e)$  versus the threshold for  $\sigma=0.5; 1; 2; 4, A=1$

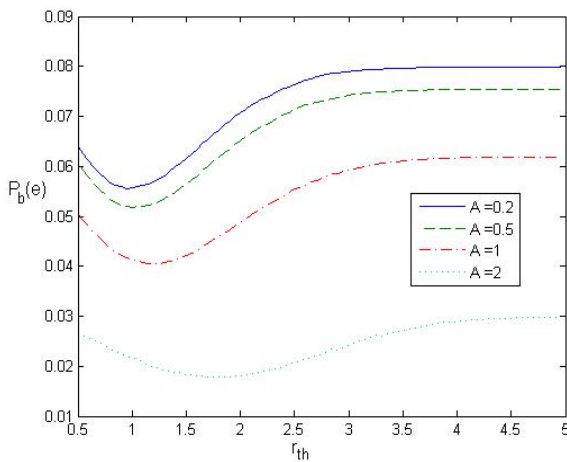


Figure 15. The bit error rate  $P_b(e)$  versus the threshold for  $\sigma=1, A=0.2; 0.5; 1; 2$

The bit error rate curves versus the threshold are given in Figures 14. and 15. It is evident from these Figures that bit error rate is less for bigger signal amplitude and variance  $\sigma$ , what is in good coincidence with theoretical recognition.

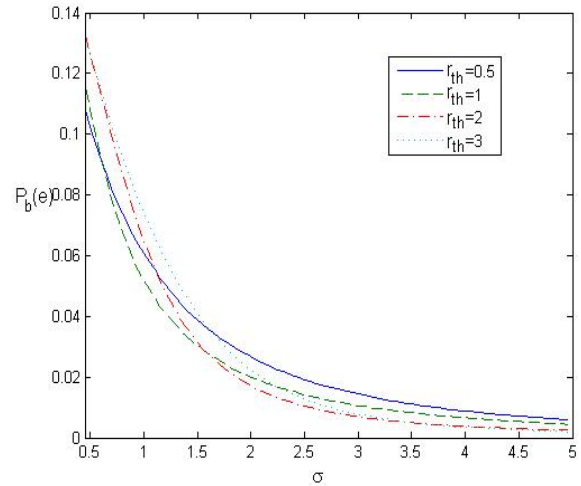


Figure 16. The bit error rate  $P_b(e)$  versus variance  $\sigma$  for  $r_T=0.5; 1; 2; 3, A=0.5$

The bit error rate curves versus variance  $\sigma$ , for different values of the threshold, are given in Figure 16. The bit error rate becomes bigger for less values of the threshold when the variances  $\sigma$  is growing up.

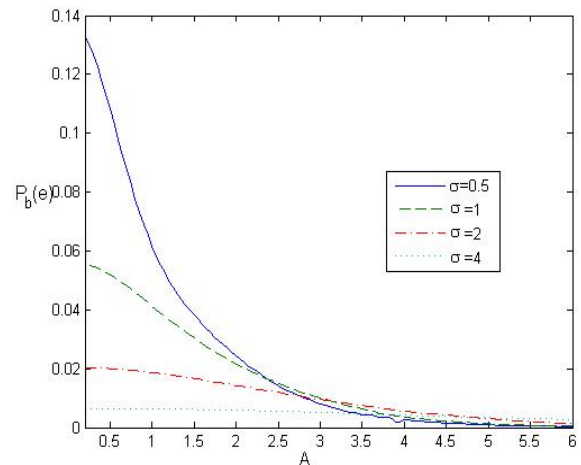


Figure 17. The bit error rate  $P_b(e)$  versus signal amplitude  $A$  for  $r_T=1, \sigma=0.5; 1; 2; 4$

The bit error rate curves versus signal amplitude  $A$ , for different values of the variance  $\sigma$ , are given in Figure 17. The bit error rate is bigger for less values of the signal amplitude  $A$  when the variances  $\sigma$  is less. The curves become wider when variance  $\sigma$  is growing up, and the bit error rate is reduced.

## V. CONCLUSION

It is known that the level crossing rate, the outage probability, the average time of fade duration and the bit error rate of combiner output signal are important system performances. In this paper these performances for the dual branch SSC combiner output signal in the presence of Rice fading are integrated and results are shown graphically for different decision threshold values, variances and signal amplitudes. Also, the analysis of the parameters influence on the system performances is done.

In the future work the number of branches could be enlarge and an analysis could be done. Also, the performances of the SSC combiner output signal in the presence of Weibull and Hoyt fading could be determined.

## REFERENCES

- [1] D. Krstić, M. Stefanović, P. Nikolić, S. Jovković, Č. Stefanović, "The Outage Probability and Fade Duration of the SSC Combiner Output Signal in the Presence of Rice fading", Proc. The Fifth Advanced International Conference on Telecommunications, AICT 2009, Venice/Mestre, Italy, May 24-28, 2009.
- [2] M. K. Simon, M. S. Alouni, Digital Communication over Fading Channels, Second Edition, Wiley Interscience, New Jersey, str. 586, 2005.
- [3] W. C. Jakes, Microwave Mobile Communication, 2nd ed. Piscataway, NJ: IEEE Press, 1994.
- [4] A. Annamalai, C. Tellambura, V. K. Bhargava, "Error performance of M-ary QAM with MRC diversity reception in a Nakagami fading channel", Proc. IEEE Int. Symp. Wireless Communications Dig., p.44, May 1998.
- [5] D. Krstić, M. Stefanović, "The statistical characteristics of the MRC diversity system output signal", Electronics and Electrical Engineering, No.1(73), pp. 45-48, January 2007.
- [6] K. Noga, "The performance of binary transmission in slow Nakagami fading channels with MRC diversity", IEEE Trans, Commun., vol. 46, pp. 863-865, July 1998.
- [7] K. Sivanesan, N. C. Beaulieu, "Exact BER analysis of bandlimited BPSK with EGC and SC diversity in cochannel interference and Nakagami fading", IEEE Commun. Lett., vol. 8, pp. 623-625, Oct. 2004.
- [8] D. Krstić, G. Stamenović, P. Nikolić, M. Stefanović, "Statistical Characteristics of Output Signal from Dual Diversity SC Combiner for Demodulation of BPSK Signals", Proc. International Scientific Conference UNITECH'08, Gabrovo, Bulgaria, 21-23. November 2008.
- [9] M. Stefanović, D. Krstić, J. Anastasov, S. Panić, A. Matović, "Analysis of SIR-based Triple SC System over Correlated  $\alpha$ - $\mu$  Fading Channels", Proc. The Fifth Advanced International Conference on Telecommunications, AICT 2009, Venice/Mestre, Italy, May 24-28, 2009.
- [10] M. S. Alouni, and M. K. Simon, "Postdetection Switched Combining- A simple Diversity Scheme With Improved BER Performance", IEEE Trans. on Commun., vol. 51, No 9, September 2003, pp.1591-1602.
- [11] A. A. Abu-Dayya and N. C. Beaulieu, "Analysis of switched diversity systems on generalized - fading channels", IEEE Trans. Commun., vol. 42, 1994, pp. 2959-2966.
- [12] Y. C. Ko, M. S. Alouni and M. K. Simon, "Analysis and optimization of switched diversity systems", IEEE Trans. Veh. Technol., vol. 49, 2000, pp.1569-1574.
- [13] C. Tellambura, A. Annamalai and V. K. Bhargava, "Unified analysis of switched diversity systems in independent and correlated fading channels", IEEE Trans. Commun., vol. 49, 2001, pp. 1955-1965.
- [14] A. A. Abu-Dayya and N. C. Beaulieu, "Switched diversity on microcellular Ricean channels", IEEE Trans. Veh. Technol., vol. 43, 1994, pp. 970-976.
- [15] M. Č. Stefanović, D. S. Krstić, P. Nikolić, S. Jovković and D. M. Stefanović, "The Performances of the SSC Combiner Output Signal in the Presence of Nakagami-m Fading", International Journal of Communications, Issue 1, Volume 2, pp. 37-44, 2008, ISSN:1998-4480, <http://www.naun.org/journals/communications/c-32.pdf>.
- [16] D. Krstić, P. Nikolić, M. Matović, A. Matović, M. Stefanović, "The Performances of the SSC Combiner Output Signal in the Presence of Log-Normal Fading", WSEAS Transactions on Communications, ISSN:1109-2742, Issue 1, Volume 8, January 2009, <http://www.worldses.org/journals/communications/communications-2009.htm>.
- [17] D. Krstić, P. Nikolić, M. Petrović, I. Temelkovski, Z. Milić, "Level Crossing Rate of the SSC Combiner Output Signal in the Presence of Rayleigh Fading", Proc. 52. Conference of ETRAN, Palić, Serbia, 8-12. june 2008. (in serbian)
- [18] D. Krstić, M. Stefanović, S. Jovković, P. Nikolić, "The joint probability density function of the SSC combiner with two inputs output signal in the presence of Rice fading", Proc. International Scientific Conference UNITECH'06, Gabrovo, Bulgaria, 24-25. November 2006.
- [19] P. Nikolic, M. Stefanovic, D. Krstic, P. Milacic, S. Jovkovic, "Level Crossing Rate of the SSC Combiner Output Signal in the Presence of Rice Fading", 17th International Electrotechnical and Computer Science Conference ERK 2008, Portorož, Slovenia, 29.september - 1. oktober 2008,
- [20] S.O.Rice, "Statistical properties of a sine wave plus random noise" Bell Syst.Tech.J,vol.27,Jan.1948,pp109-157.
- [21] J.W. Craig, "A new, simple and exact result for calculating the probability of error for two-dimensional signal constellations," IEEE MILCOM'91 Conf. Rec., Boston, MA, pp. 25.5.1-25.5.5.
- [22] M. K. Simon, S. M. Hinedi, and W. C. Lindsey, "Digital Communication Techniques - Signal Design and Detection. Englewood Cliffs", NJ: PTR Prentice-Hall, 1995.

# Dynamic Power and Bit Allocation Scheme for Spectral Efficiency Maximization in Cognitive Multiband OFDM UWB Systems

Liaoyuan Zeng  
Wireless Access Research Center  
University of Limerick  
Limerick, Ireland  
Email: liaoyuan.zeng@ul.ie

Sean McGrath  
Wireless Access Research Center  
University of Limerick  
Limerick, Ireland  
Email: sean.mcgrath@ul.ie

Eduardo Cano  
Institute for the Protection and  
Security of the Citizen  
Joint Research Center  
European Commission  
Ispra, Italy  
Email: eduardo.cano@jrc.ec.europa.eu

**Abstract**—A novel dynamic power and bit allocation scheme for spectral efficiency maximization in the Cognitive Ultra Wideband radio system is presented in this paper. A new bit error rate expression is derived based on approximating a sum of independent log-normal random variables as a single log-normal random variable using the Fenton-Wilkinson method in order to analyze the spectral efficiency in the UWB multipath channel. A series of  $M$ -ary quadrature amplitude modulation zones can be generated over each UWB subcarrier by manipulating the BER expression. The total transmitted power is optimally distributed among the UWB subcarriers for the use of those zones with a maximum  $M$  on each subcarrier. The power and bit allocation is divided into primary allocation and advanced allocation for efficient implementation. The performance of the dynamic allocation algorithm is analyzed over different UWB fading channels. The results show that the spectral efficiency of the system is significantly improved by an optimal power and bit allocation techniques.

**Keywords**—Ultra Wideband; Multiband Orthogonal Frequency Division Multiplexing; Bit Error Rate; Cognitive Radio.

## I. INTRODUCTION

Radio spectrum is a scarce resource, both dynamic power allocation and adaptive spectrum sharing through cognitive radios can significantly enhance the spectrum utilization in a wireless network [1][2]. The principle behind cognitive radio consists of defining and developing technologies that can enable a radio device to sense the states of the frequency bands and adapt its internal states to statistical variations in the incoming RF stimuli by making corresponding changes in certain operation parameters in real-time. Thus, a cognitive (unlicensed/secondary) system can detect and access the temporarily-unused spectrum very rapidly without interfering with the primary (licensed) systems (e.g., WiMAX).

Several physical-layer radio platforms have been suggested for cognitive radio networks, one of the leading candidates is Multiband Orthogonal Frequency Division Multiplexing (MB-OFDM) Ultra Wideband (UWB) system [3][4]. UWB systems use signals with a fractional bandwidth greater than 0.20 or occupy a minimum of 500 MHz (-10 dB) bandwidth in

the 3.1–10.6 GHz frequency band with a maximum mean Power Spectral Density (PSD) of -41.3dBm/MHz [5]. The UWB bandwidth is subdivided into a number of orthogonal subcarriers (subchannels) with bandwidth of each less than the channel coherence bandwidth. Hence, the Intersymbol Interference (ISI) caused by multipath fading is minimized when the information is transmitted over different subcarriers. Furthermore, the MB-OFDM scheme can significantly enhance the flexibility and ease of dynamically allocating unused spectrum in cognitive UWB radio systems [4].

A novel dynamic power and bit allocation scheme for spectral efficiency maximization in the cognitive MB-OFDM UWB radio systems in a multipath fading channel is presented in this paper. This work is based on our previous work [1] which did not integrate the cognitive radio technology into the UWB systems. Furthermore, for an in-depth spectral efficiency analysis of UWB multipath channel, a new Bit Error Rate (BER) expression is derived based on approximating a sum of independent log-normal random variables as another log-normal random variable using the Fenton-Wilkinson method [6]. The optimization of the spectral efficiency is under the constraints in probability of detection and false alarm, transmission PSD and BER. The objective is to maximize the number of the information bits loaded in the UWB subcarriers (each with different levels of fading [7]) by optimally allocating the available total transmitted power while guaranteeing a sufficient protection to the primary users.

By exploiting the channel conditions, a cognitive UWB system can opportunistically access the temporarily-unused spectrums and implement the optimal power and bit allocation schemes. The fraction of time for UWB data transmission is constrained by the spectrum sensing period and the probability that the primary user is transmitting or receiving within the spectrum of the UWB subcarriers. It is assumed that this probability follows a Poisson process. The information bits assigned in each subcarrier are modulated using  $M$ -ary Quadrature Amplitude Modulation (M-QAM) modulation. Thus, it is required to use the modulation scheme with the

maximum  $M$  in the subcarrier to maximize the spectral efficiency.

The paper is organized as follows. In Section II, a literature review of the spectral efficiency optimization in cognitive multicarrier systems is presented. Next, the system model is discussed in Section III, including the discussion of the UWB multipath propagation, the multiband OFDM scheme and the cognitive UWB radio systems. In Section IV, a new in-depth BER performance analysis is carried out. On the basis of the BER analysis, the system spectral efficiency is analyzed in Section V. Then, the design of the dynamic power and bit allocation algorithm is provided in Section VI. The analysis of the simulation results is carried out in Section VII. Finally, conclusions are presented in Section VIII.

## II. LITERATURE REVIEW

The discussion of the UWB cognitive radio systems optimization with respect to spectrum sensing and dynamic spectrum sharing has been treated extensively in the literature dedicated to wireless systems and theory [3][8][9][10]. As an optimization problem in multicarrier transmission systems, the spectral efficiency maximization problem (in terms of how to optimally allocate bits and power to UWB subcarriers) is originally a non-convex integer-programming optimization problem which is generally NP-hard [9]. The common solution is either to relax this non-convex optimization problem into a convex optimization problem or to use some metaheuristic algorithm such as greedy algorithm to approximate the optimal solution [9][11].

The theoretical capacities achieved by the cognitive Impulse Radio (IR) UWB systems with constraints in outage probability of the primary users were studied in [3]. The authors in [4] proposed a power allocation scheme using Lagrange formulation to maximize the total transmission capacity of the OFDM-based cognitive users. In [12], the effects of the multipath fading channel on the choice of the transmitted power level were taken into account for the design of the cognitive power control strategies for system ergodic capacity maximization. These addressed the fundamental channel rate limits of the cognitive radio systems from an information theory perspective.

Furthermore, in the derivation of the MB-OFDM UWB BER expression in [13][14], the authors assumed that the multipath gain coefficients of the UWB channel model have a statistically independent Gaussian distribution with zero mean and variances. Authors in [15] made similar assumptions and approximated the UWB channel frequency response to a Rayleigh fading channel. In this paper, a more accurate BER expression is derived based on the log-normal distribution of the UWB multipath gain coefficient. The UWB channel measurement studies [5][16][17][18][19] have suggested that the log-normal distribution can more accurately reflect the measurement data.

## III. SYSTEM MODEL

This section provides a review of the MB-OFDM UWB systems and cognitive UWB radio systems, and specifically focuses on the introduction of the MB-OFDM schemes.

### A. UWB Signal

The MB-OFDM UWB transmitted signal of the node  $u$  is represented by

$$x^{(u)}(t) = \sum_{i=-\infty}^{+\infty} \frac{1}{T_S} \sum_{n=0}^{N_{FFT}-1} c_{n,i} g(t - iT'_S) e^{j2\pi n(t - iT'_S)/T_S}, \quad (1)$$

where  $T_S$  is the duration of the useful OFDM symbol and  $N_{FFT}$  is the number of subcarriers and also the number of points of the Inverse Discrete Fourier Transform (IDFT). The total duration of the OFDM symbol is computed as  $T'_S = T_S + T_{cp} + T_G$  where  $T_{cp}$  is the duration of the cyclic prefix for ISI mitigation and  $T_G$  is the duration of the guard interval that ensures a smooth transition between two consecutive OFDM symbols. The data sequence in (1) is expressed as  $\mathbf{c} = c_{0,i}, c_{1,i}, \dots, c_{n,i}, \dots, c_{N-1,i}$  being  $i$  the OFDM symbol index and  $n$  the subcarrier index. Finally, the function  $g(t)$  represents the unitary rectangular pulse of duration  $T_S$ . In this work, it is assumed that each data symbol is normalized to have unit energy.

### B. UWB Channel

In this work, the UWB multipath channel is modeled by using the Saleh-Valenzuela (S-V) model which captured the clustering phenomenon through practical channel measurements [5]. This UWB channel model is assumed to be linear time-invariant during the transmission of a data packet. The impulse response of the UWB multipath channel with  $J$  multipath components is expressed as

$$\mathbf{h}(t) = \sum_{j=0}^J \alpha_j \delta(t - T_j), \quad (2)$$

where  $\alpha_j$  are the multipath gain coefficients which denotes the amplitude of multipath components subjected to log-normal distribution [16].

The multipath gain coefficients  $\alpha_j$  are given by:

$$\alpha_j = p_j \xi_j, \quad (3)$$

where  $p_j$  is equiprobable  $\pm 1$  to account for signal inversion due to reflections,  $\xi_j$  reflects the log-normal fading associated with the  $j$ th multipath component. This log-normal variable can be expressed in terms of Gaussian random variable as:

$$\xi_j = 10^{\frac{x_j}{20}}, \quad (4)$$

where  $x_j$  is a normal random variable with mean  $\mu_j$  and variance  $\sigma^2$ . The  $\mu_j$  is given by:

$$\mu_j = \frac{10 \ln(\Omega_0) - 10 \frac{T_j}{T}}{\ln(10)} - \frac{(\sigma^2) \ln(10)}{20}, \quad (5)$$

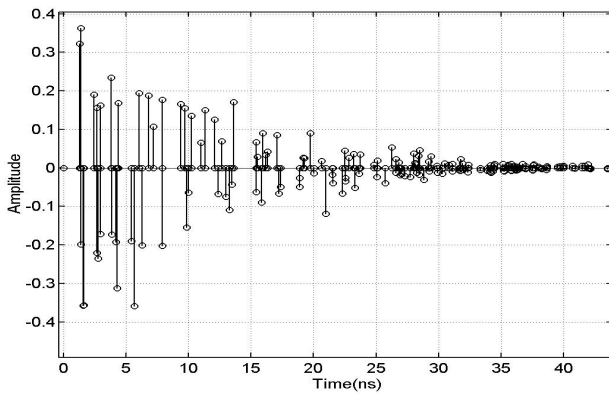


Fig. 1. Impulse Response over CM3

where  $\Omega_0$  is the mean energy of the first arrived multipath component, and  $\Gamma$  is the signal decay factor.

The order of  $L = J$  is determined by  $L = T_d/T_s$ , where  $T_d$  is the maximum delay spread of the UWB channel, and  $T_s$  is the M-QAM symbol period. Hence, it is assumed that the delay between the multipath components is  $T = \tau = T_s$  for the reasons of both analytical convenience and sampling processing at the receiver [20]. This assumption is well suited to dense scattering environments. The discrete time version of  $\mathbf{h}(t)$  can be expressed as  $\mathbf{h} = \mathbf{h}(t)|_{t=lT_s} = \{h(0), h(1), \dots, h(L-1)\}$ , where  $h(l)$  ( $l \in [0, L-1]$ ) is the impulse response of the  $l$ th path.

There are four types of UWB Channel Models (CMs) defined based on the practical measurements of the key channel parameters such as mean excess delay and Root Mean Square (RMS) delay spread [5]. A channel impulse response realization for CM3 is represented in Figure 1.

### C. Multiband-OFDM Scheme

In MB-OFDM scheme [5], the 3.1–10.6 GHz UWB bandwidth is divided into fourteen sub-bands, each with 528 MHz. An OFDM symbol is transmitted within one sub-band. In each sub-band, a total number of 128 orthogonal subcarriers are used for data transmission.

In a UWB transmitter, the outgoing data packet is first encoded using punctured convolutional code. Then, the coded data is interleaved and modulated into a series of complex M-QAM symbols  $\mathbf{S}_n = [S_n(0), S_n(1), \dots, S_n(N-1)]^T$  of length  $N = 128$ , where column vector  $\mathbf{S}_n$  represents the  $n$ th transmitted OFDM symbol, and  $S_n(i)$  ( $i \in [0, N-1]$ ) stands for a single M-QAM symbol. Note that the system performance is not addressed with the Forward Error Correction (FEC) coding in this paper. It is assumed that the data packet transmitted is not encoded. The discrete  $N$ -point Inverse Fast Fourier Transform (IFFT) is employed to perform the subcarrier modulation. Thus, the frequency domain signal  $\mathbf{S}_n$  is transformed into a real-valued time domain signal  $\mathbf{s}_n = \mathbf{F}\mathbf{S}_n = [s_n(0), s_n(1), \dots, s_n(N-1)]^T$ , where  $\mathbf{F}$  is a square IFFT matrix with  $(i, k)$ th entry as

$\mathbf{F}(i, k) = \frac{1}{\sqrt{N}} e^{j2\pi ik/N}$  ( $i, k \in [0, N-1]$ ). Since the subcarriers are orthogonal to each other, there will be no Inter-Carrier-Interference (ICI) between the  $s_i$  modulated subcarriers. Note that the transmission channel modeled as a linear time invariant channel during the transmission of a data packet.

The  $i$ th received time domain sequence  $\mathbf{r}_i = [r_i(0), r_i(1), \dots, r_i(N-1)]^T$  is the result of the linear convolution between  $\mathbf{h}(l)$  and  $\mathbf{s}_i = [s_i(0), s_i(1), \dots, s_i(N-1)]^T$

$$r_i(n) = \sum_{l=0}^{L-1} s_i(l)h(n-l) + \eta(n). \quad (6)$$

Thus, the  $i$ th received frame  $\mathbf{r}_i$  can be expressed as

$$\mathbf{r}_i = \mathbf{h}\mathbf{s}_i + \eta_i, \quad (7)$$

where  $\mathbf{h}$  is a  $N \times N$  Toeplitz matrix which can transfer the above convolution operation into a matrix multiplication [7], i.e.

$$\mathbf{h} = \begin{pmatrix} h(0) & 0 & 0 & \dots & 0 \\ h(1) & h(0) & 0 & \dots & 0 \\ \vdots & \vdots & \vdots & \vdots & \vdots \\ h(L-1) & h(L-2) & \dots & \dots & 0 \\ \vdots & \vdots & \vdots & \vdots & \vdots \\ 0 & 0 & h(L-1) & \dots & h(0) \end{pmatrix}. \quad (8)$$

However, if the  $i$ th frame  $\mathbf{s}_i$  is transmitted immediately after the  $i-1$ th frame  $\mathbf{s}_{i-1}$ , the first  $L-1$  symbols of  $\mathbf{s}_i$  will be corrupted by the delayed version of the last  $L$  symbols of  $\mathbf{s}_{i-1}$ . When the  $(N-L+1)$ th symbol  $s_{i-1}(N-L+1)$  of  $\mathbf{s}_{i-1}$  is transmitted at time  $(N-L+1)T_s$ , the delayed component of  $s_{i-1}(N-L+1)$  will last  $(L-1)T_s$  and corrupt with the first symbol of  $\mathbf{s}_i$  at time  $LT_s$ . Thus, the delayed component of the last symbol  $s_{i-1}(N-1)$  transmitted at time  $(N-1)T_s$  will corrupt with the first  $(L-1)$ th symbol of  $\mathbf{s}_i$ . This type of corruption is so-called Inter-Frame-Interference (IFI) or Inter-Block-Interference (IBI).

Hence, the received frame is expressed as

$$\mathbf{r}_i = \mathbf{h}\mathbf{s}_i + \mathbf{h}_d\mathbf{s}_{i-1} + \eta_i, \quad (9)$$

where  $\mathbf{h}_d$  is also a  $N \times N$  Toeplitz matrix

$$\mathbf{h}_d = \begin{pmatrix} 0 & \dots & h(L-1) & \dots & h(1) \\ 0 & \dots & 0 & \dots & 0 \\ \vdots & \vdots & \vdots & \vdots & \vdots \\ 0 & \dots & 0 & \dots & h(L-1) \\ \vdots & \vdots & \vdots & \vdots & \vdots \\ 0 & \dots & 0 & \dots & 0 \end{pmatrix}. \quad (10)$$

To eliminate the corruption between received frames, the time domain sequence  $\mathbf{s}_n$  is tail attached by a zero-padded suffix (ZPS) of length  $L$  [5]. More importantly, appending the ZPS can manipulate the linear convolution between  $\mathbf{s}_n$  and the UWB channel impulse response  $\mathbf{h}(t)$  into a circular convolution by implementing the time-domain aliasing

[21]. Thus, the  $i$ th received frequency domain signal,  $\mathbf{R}_n = [R_n(0), R_n(1), \dots, R_n(N-1)]^T$ , can be expressed as

$$\mathbf{R}_n = \mathbf{F}^{-1} \tilde{\mathbf{H}} \mathbf{F} \mathbf{S}_n + \eta_n, \quad (11)$$

where  $\eta_n$  is the noise figure, and  $\tilde{\mathbf{H}} = \mathbf{R} \mathbf{h} \mathbf{Z}$  is a  $N \times N$  circulant matrix with its  $(i, l)$ th entry given by  $h((i-l) \bmod N)$ , where  $\mathbf{R}$  and  $\mathbf{Z}$  are the ZPS attaching and removing matrix [7]. The expression  $\mathbf{F}^{-1} \tilde{\mathbf{H}} \mathbf{F} = \mathbf{H} = \text{diag}[H(0), H(1), \dots, H(N-1)]$  is a  $N \times N$  diagonal matrix. By taking the Fourier transform of  $h(t)$ , the transfer function of the  $i$ th MB-OFDM UWB subcarrier  $H(i)$  ( $i \in [0, N-1]$ ) can be obtained.  $H(i)$  is specified as

$$H(i) = H(2\pi i/N) = \sum_{l=0}^{L-1} h(l) e^{-j2\pi i l/N}, \quad (12)$$

It is assumed that  $H(i)$  is known at the receiver. Figure 2 shows an example of channel frequency response for CM3.

#### D. Cognitive MB-OFDM UWB Systems

In this paper, it is considered that the cognitive UWB systems can only access the spectrum of the subcarrier when the spectrum is not occupied by any primary user. Thus, the spectrum sensing process determines the probability that a subcarrier is utilized by the cognitive UWB system. The key parameters for evaluating the performance of sensing are the probability of a false alarm  $P_f$  and the probability of detection  $P_d$  [22]. An energy detection method is adopted in this work, since energy detection does not need any information of the signal to be detected and is robust to unknown dispersed channel and fading [23].

The amount of time needed for a successful spectrum sensing is denoted as a sensing period  $\tau_s$ . The fraction of time for data transmission is limited by the value of  $\tau_s$  as  $\alpha = \frac{T_{txop} - \tau_s}{T_{txop}}$ , where  $T_{txop}$  is a pre-defined transmission period in the UWB MAC layer for different Access Categories (ACs) [24], called Transmission Opportunity (TXOP). An application with  $T_{txop} = 512 \mu\text{s}$  (ACs) is chosen in this work to be activated in the cognitive UWB system.

For an energy detector, the required sensing period  $\tau_{s_i}$  according to the target probability of false alarm  $\tilde{P}_f$  and probability of detection  $\tilde{P}_d$  can be determined as

$$\tau_{s_i} = \frac{2}{\gamma_p^2 f_s} (Q^{-1}(\tilde{P}_f) - Q^{-1}(\tilde{P}_d))^2, \quad (13)$$

where  $Q(z) = \int_z^\infty \frac{1}{\sqrt{2\pi}} e^{-y^2/2} dy$  is the complementary distribution function of the standard Gaussian,  $\gamma_p$  is the received Signal-To-Noise Ratio (SNR) of the primary user signals ( $\text{SNR}_p$ ) at the cognitive UWB user, and  $f_s$  is the UWB receiver sampling frequency [23].

#### IV. BER PERFORMANCE ANALYSIS

The averaged probability of error of MB-OFDM UWB system is computed by integrating the error probability in Additive White Gaussian Noise (AWGN) channel over the UWB fading distribution. In (11), it is demonstrated that the

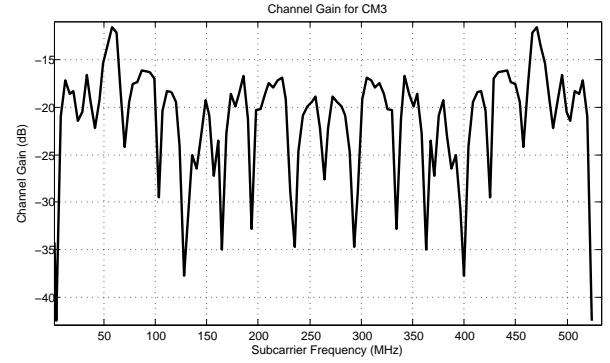


Fig. 2. Frequency response over CM3

amplitude variations in the received signal are due to the characteristics of the UWB multipath channel. Since  $\alpha_j$  in (2) is modeled as a series of independent (uncorrelated) log-normal random process, the distribution of the  $|H(i)|$  at the  $i$ th subcarrier can be derived from the manipulating the sum of independent log-normal variables  $\alpha_j$ . Although an exact closed-form expression for the probability density function (PDF) of a sum of independent log-normal random variables does not exist, the superposition of log-normal variables can be well approximated by a new log-normal distribution using Fenton-Wilkinson method [6].

It is illustrated in (4) that the  $j$ th random variable  $x$  has the Gaussian distribution

$$p_X(x) = \frac{1}{\sqrt{2\pi}\sigma_x} e^{-\frac{(x-\mu_x)^2}{2\sigma_x^2}}, \quad (14)$$

where  $[\mu_x, \sigma_x]$  are the mean and standard deviation of  $x$ . Then, the probability distribution of  $\xi_j = 10^{x_j/20}$  can be expressed as a log-normal distribution:

$$p_\xi(\varepsilon) = \frac{20/\ln 10}{\varepsilon \sigma_x \sqrt{2\pi}} e^{-\frac{(20/\ln 10 \ln \varepsilon - \mu_x)^2}{2\sigma_x^2}}. \quad (15)$$

The received signal amplitude  $|H(i)| = r$  on the  $i$ th subcarrier has the distribution of the sum of log-normal random variables  $\alpha_j$ . There is a general consensus that the sum of independent log-normal random variables can be approximated by another log-normal random variable with appropriately chosen parameters [25][26]. Therefore,

$$p(r) = \sum_{j=1}^J 10^{\xi_j/20} = 10^{Z/20} = p(\hat{r}), \quad (16)$$

where  $Z$  is a Gaussian random variable with mean  $\mu_z$  and variance  $\sigma_z^2$ .

In Fenton-Wilkinson method, the value of  $\mu_z$  and  $\sigma_z^2$  can be calculated by

$$\mu_z = \xi^{-1} \left( \frac{\sigma_\xi^2 - \sigma_z^2}{2} + \ln \left( \sum_{j=1}^J e^{\hat{\mu}_j} \right) \right), \quad (17)$$

$$\sigma_z^2 = \xi^{-2} \left( \ln \left( (e^{\sigma_\xi^2} - 1) \frac{\sum_{j=1}^J e^{2\hat{\mu}_j}}{(\sum_{j=1}^J e^{\hat{\mu}_j})^2} + 1 \right) \right), \quad (18)$$

where  $\xi = \ln 10 / 20$ ,  $\sigma_\xi^2 = \xi^2 \sigma^2$ , and  $\hat{\mu}_j = \xi \mu_j$ .

Therefore, the distribution of the received signal amplitude  $r$  can be expressed as

$$p(r) = \frac{20/\ln 10}{r\sigma_z\sqrt{2\pi}} e^{-\frac{(20\log(r)-\mu_z)^2}{2\sigma_z^2}}. \quad (19)$$

From (19), the distribution of the received SNR per symbol  $p_{\gamma_s}(\gamma)$  can be expressed as

$$p_{\gamma_s}(\gamma) = \frac{10/\ln 10}{\gamma\sigma_z\sqrt{2\pi}} e^{-\frac{(10\log(\gamma N_0/E_s)-\mu_z)^2}{2\sigma_z^2}}. \quad (20)$$

For more convenient calculation of  $p_{\gamma_s}(\gamma)$ , the parameter  $N_0/E_s$  can be replaced with  $E(r^2)\gamma/\bar{\gamma}_s$  in the equation above since the average SNR per symbol  $\bar{\gamma}_s = E(r^2)\frac{E_s}{N_0}$ , where  $E(r^2)$  is the mean value of the signal power distribution. The expression of  $E(r^2)$  can be easily derived by manipulating (19) and expressed as

$$E(r^2) = E(R) = e^{\frac{\mu_z}{10/\ln 10} + \frac{\sigma_z^2}{2*(10/\ln 10)^2}}. \quad (21)$$

The averaged probability of symbol error and bit error in UWB multipath fading channel can be computed by averaging the error probability in AWGN  $P_s(\gamma)$  over the UWB fading distribution  $p_{\gamma_s}(\gamma)$  [27]:

$$\bar{P}_s = \int_0^\infty P_s(\gamma)p_{\gamma_s}(\gamma)d\gamma. \quad (22)$$

In arriving at the error rate results in equations, it is assumed that timing and frequency synchronization is perfect. In such a case, the expressions in equations should be viewed as representing the best achievable performance in the presence of log-normal fading.

For rectangular M-ary QAM modulation with coherence detection, the BER calculation in AWGN channel is expressed as

$$P_b(\gamma) = \frac{4(\sqrt{M}-1)}{\sqrt{M}\log_2 M} Q\left(\sqrt{\frac{3\gamma_b \log_2 M}{M-1}}\right), \quad (23)$$

where  $Q(x) = \frac{1}{\sqrt{2\pi}} \int_x^\infty e^{-t^2/2} dt$ ,  $x \leq 0$ .

By replacing the (23) into (22), the BER performance for different M-QAM modulations in CM1 and for QPSK in different UWB channel models is shown in Figure 3 and Figure 4, respectively. For comparison purposes, the BER curves in AWGN channel and Rayleigh fading channel are also provided. It is observed from the figures that the BER performance for QPSK in UWB fading channel is better than that in Rayleigh fading channels. Furthermore, the BER performance is better in the UWB channel models with less severe multipath fading [5][28].

### V. SPECTRAL EFFICIENCY ANALYSIS

On the basis of the analysis of the BER performance in MB-OFDM UWB systems, the spectral efficiency with equal power allocation and equal bit allocation is analyzed in this section. The objective of this section is to demonstrate the motivation of proposing a dynamic power and bit allocation algorithm. The performance analyzed in this section will be compared

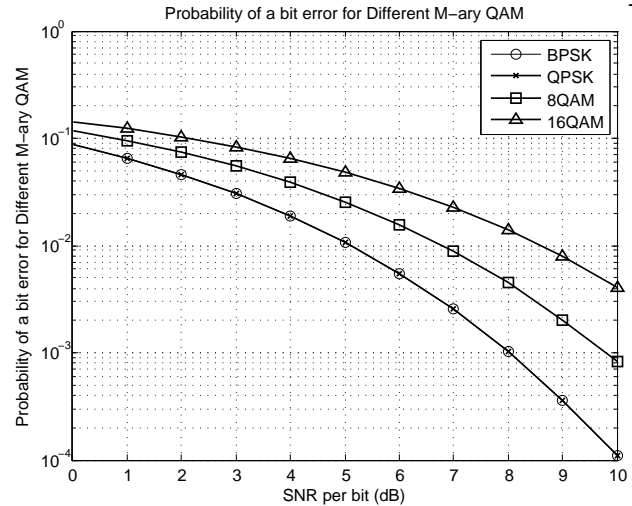


Fig. 3. BER for Different MQAM in CM1

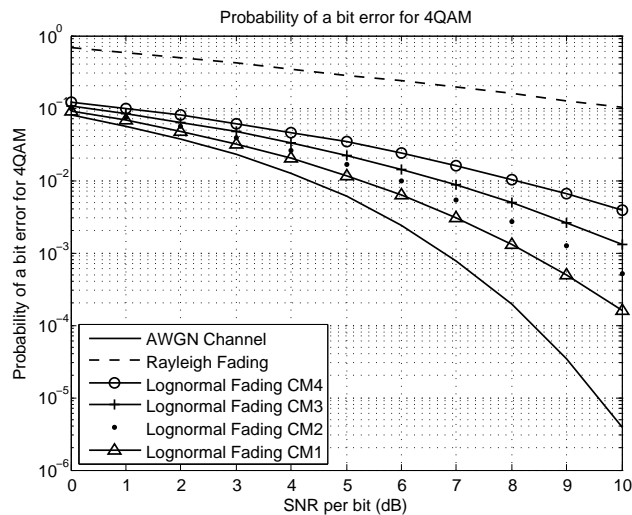


Fig. 4. BER for Different Channel Models

with the performance of the proposed allocation algorithm in the next section.

In the MB-OFDM UWB system, the total available transmitted power can be denoted as  $P_{av}$ . Since the maximum mean PSD for UWB system is limited to -41.3dBm/MHz, the average maximum allowable transmitted power of the system  $P_{max}$  can be approximated as

$$P_{max} \text{ (dB)} = -41.3 \text{ dBm/MHz} + 10\log_{10}(f_H - f_L), \quad (24)$$

where  $f_H$  and  $f_L$  denote the higher and lower frequency of the operating bandwidth in MHz [5]. When the total available transmitted power is  $P_{av} = P_{max}$ , it is intuitively clear that to maximize the total number of bits which can be allocated into a subband under the power and BER constraints, the optimal strategy should be to equally allocate the transmitted power  $P_t(i) = \bar{P}_{max} = P_{av}/N$  to each subcarrier [27]. The spectral efficiency performance with equal power allocation is analyzed when the available power  $P_{av} < P_{max}$ .

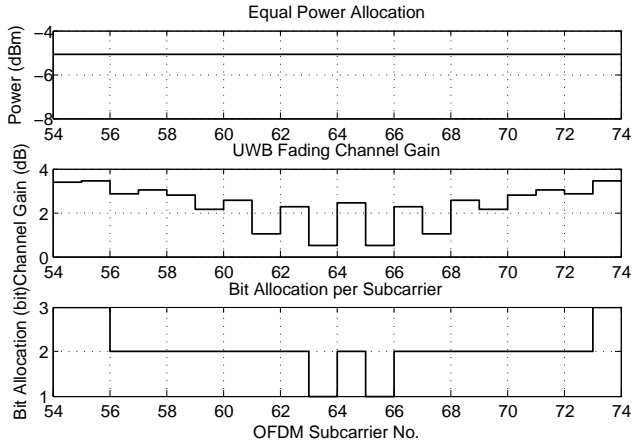


Fig. 5. Bit Allocation in CM1

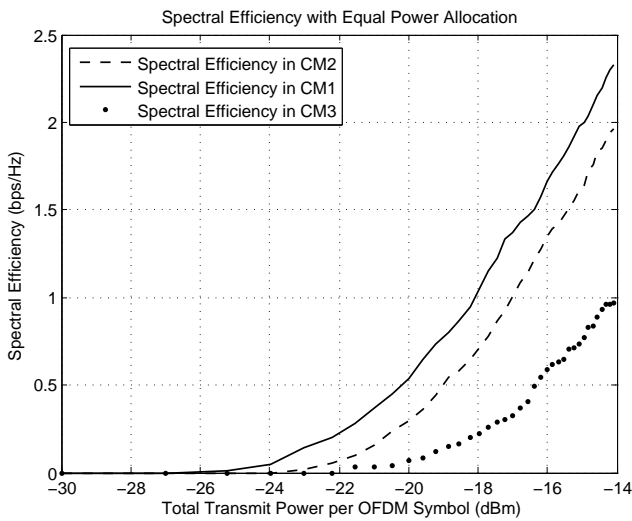


Fig. 6. Spectral Efficiency in CM1

The data bits are dynamically allocated in the OFDM UWB transmitter when the total transmitted power is equally allocated, as illustrated in Figure 5. In this figure, it is observed that there are more bits being allocated to the subcarriers with higher channel gain (less channel multipath fading). Furthermore, the performance of the spectral efficiency in CM1 to CM3 as a function of the total transmitted power per OFDM symbol is illustrated in Figure 6. It can be seen that the spectral efficiency is increased exponentially as the transmitted power increases. The allocation algorithm discussed in the next section can significantly increase the spectral efficiency under the constraints from the primary users while keep the number of iterations to convergence small.

## VI. DYNAMIC POWER AND BIT ALLOCATION SCHEME

In this section, the proposed dynamic power and bit allocation algorithm is presented. The spectral efficiency maximization algorithm is divided into four sections. These are: spectrum sensing, M-QAM zones generation, primary power and bit allocation and advanced power and bit allocation.

TABLE I  
SPECTRAL EFFICIENCY MAXIMIZATION ALGORITHM

Step	Operations
Step 1	Sense the operating channel, and access the available subcarriers of which the target $\tilde{P}_f$ and $\tilde{P}_d$ are achieved for M-QAM zones generation in step 2.
Step 2	Generate a series of M-QAM zones in each available subcarrier by determining the minimum required transmitted power $P_k(i)$ of the $i$ th subcarrier for reliable reception of the $k$ th order M-QAM symbol.
Step 3	Equally allocate the total available power $P_{av}$ among all the $N$ subcarriers in a sub-band, and specify the order of the M-QAM to use in each subcarrier by identifying the M-QAM zones $Z_k(i)$ where $P_t(i)$ falls in.
Step 4	Collect the excessively allocated power in step 3, and iteratively allocate the collected power using greedy algorithm to the subcarrier that requires the least additional power for using a higher order M-QAM while $P_t(i) < \tilde{P}_{max}$ .

In the proposed algorithm, the steps of spectral efficiency maximization are summarized in Table I and described in detail as follows.

### A. Optimization Problem Formulation

The optimization problem is formulated as follows:

$$\arg \max_{P_t(i)} \sum_{i=1}^N \mathbf{B}(i), \quad \mathbf{B}(i) \subseteq \mathbf{Z}, \quad (25)$$

subject to

$$p_e \leq \tilde{p}_e \quad (26)$$

$$0 \leq P_{av} \leq P_{max} \quad (27)$$

$$0 \leq P_t(i) \leq \tilde{P}_{max} \quad (28)$$

$$\tilde{P}_d \leq P_d \leq 1, \quad 0 \leq P_f \leq \tilde{P}_f, \quad (29)$$

where in (25), the parameter  $P_t(i)$  is the power allocated to the  $i$ th subcarrier for data transmission,  $N$  is the total number of the UWB subcarriers, and  $\mathbf{B}(i)$  is an integer number of the loaded information bits in the  $i$ th subcarrier under conditions. In (26),  $p_e$  is the BER of the system, and  $\tilde{p}_e$  is the required BER of the MB-OFDM UWB system.

It is observed from (25) to (29) that the spectral efficiency maximization problem in MB-OFDM UWB systems is a non-convex optimization problem which is NP-hard [29], since the variable  $\mathbf{B}(i)$  in the objective function (25) is limited to some integer value. To effectively solve this optimization problem, the heuristic greedy algorithm [11] is adopted in this paper.

### B. Spectrum Sensing

The spectrum sensing procedure determines the probability that a subcarrier is utilized by the cognitive UWB system. The procedure also determines the fraction of time for UWB data transmission  $\alpha_i$  in the  $i$ th subcarrier. Thus, the number of the loaded information bits in the  $i$ th subcarrier under conditions  $\mathbf{B}(i)$  in (25) can be expressed as

$$\mathbf{B}(i) = B(i)\alpha_i(1 - P_f)(1 - P(H_{1_i})), \quad (30)$$

where  $B(i)$  is the bits loaded in the  $i$ th subcarrier, and  $P(H_{1_i})$  is the probability that the primary user is transmitting

or receiving within the spectrum of the  $i$ th subcarrier. It is assumed that the value of  $P(H_{1_i})$  follow a Poisson process with intensity set to  $\lambda = 1$ , which represents the average number of transmissions per 1ms from the primary users. Hence,  $P(H_{1_i}) = p(1; \lambda T_{txop_i})$ , where  $p(x; \lambda t) = \frac{e^{-\lambda t} (\lambda t)^x}{x!}$ . For simplicity, the parameter  $P_f$  in (30) is approximated by  $P_f = \bar{P}_f$ .

### C. M-ary QAM Zones Generation

The M-QAM modulation constellation size  $M_k(i)$  is restricted to  $M_k(i) = 2^k$ , ( $k = 1, 2, 3, \dots, K$ ). The rectangular QAM is assumed when  $k > 1$  due to energy efficiency and ease of implementation [21]. It is considered that the cognitive UWB users can gather the instantaneous channel state information (CSI) of all links [27]. Thus, the minimum required transmitted power  $P_k(i)$  in the  $i$ th subcarrier for reliable reception of the  $k$ th order M-QAM symbol can be determined as discussed in Section IV.

Then, a series of M-QAM zones  $Z_k(i)$ , ( $k = 0, 1, 2, 3, \dots, K$ ) are generated by assigning

$$Z_k(i) = [P_k(i), P_{k+1}(i)) \quad k > 0 \quad (31)$$

$$Z_0(i) = [P_0(i), P_1(i)) \quad k = 0, \quad (32)$$

where  $[\cdot)$  represents a half-open interval, and  $P_0(i) = 0$  means that no transmission power is required. The  $k$ th order M-QAM will be used in the  $i$ th subcarrier when the allocated power  $P_t(i) \in Z_k(i)$ . Figure 7 shows the M-QAM zone generation. Five M-QAM zones are generated for each subcarrier. For example, the required transmitted power  $P_k(3)$  ( $k = \{1, 2, 3, 4\}$ ) in the subcarrier-3 is lower than  $P_k(2)$  in the subcarrier-2 for each  $k$ th order M-QAM due to the higher channel gain of the subcarrier-3.

### D. Primary Power and Bit Allocation

In the step 3 of the algorithm, the transmitter initially splits  $P_{av}$  equally among all the  $N$  subcarriers in a sub-band as  $P_t(i) = \bar{P}_t(i) = P_{av}/N$ . Therefore, the constellation size  $B(i)$  allocated to the  $i$ th subcarrier can be determined as

$$B(i) = \log_2(M_k)\alpha(i), \quad (33)$$

where  $\alpha(i) = \{0, 1\}$  is the allocation coefficient, and is expressed as

$$\alpha(i) = \begin{cases} 1 & P_t(i) \in Z_k(i) \\ 0 & P_t(i) \in Z_0(i). \end{cases} \quad (34)$$

An example is shown in Figure 7, where zero bit is assigned to subcarrier-1 since  $\bar{P}_t(i)$  falls into the zone-0 of subcarrier-1, while 2 bits are assigned to subcarrier-2 for 4-QAM since  $\bar{P}_t(i)$  falls into the zone-2 of subcarrier-2.

### E. Advanced Power and Bit Allocation

It is noticeable in Figure 7 that  $\bar{P}_t(i)$  of each subcarrier exceeds the required transmitted power  $P_k(i)$ . Hence, at the beginning of step 4, the transmitter decreases the allocated power  $P_t(i) = \bar{P}_t(i)$  to  $P_t(i) = P_k(i)\alpha(i)$ . The excessive

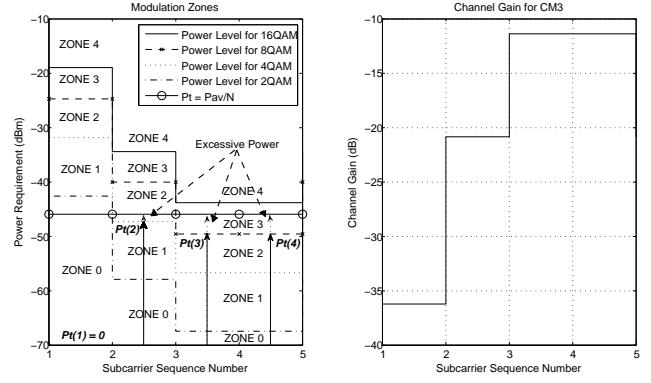


Fig. 7. M-ary QAM zone generation over CM3

allocated power  $P_m$  is collected for the advanced allocation, and is given by

$$P_m = P_{av} - \sum_{i=0}^{N-1} P_t(i). \quad (35)$$

Then,  $P_m$  is optimally distributed to the subcarriers by using the greedy algorithm to maximize the number of bits to be carried by each subcarrier [11]. Therefore, the additional power  $\Delta P_t = \{\Delta P_t(i), (i \in [0, N - 1])\}$  needed to promote the order of the M-QAM in each subcarrier is determined by

$$\Delta P_t(i) = P_{k+1}(i) - P_k(i). \quad (36)$$

Next, the  $i$ th subcarrier with the minimum  $\Delta P_t(i) = \min(\Delta P_t)$  is chosen to be promoted to use a higher order M-QAM by assigning more power and bits to this subcarrier when  $\Delta P_t(i) \leq P_m$ . Thus,  $P_t(i)$  and  $B(i)$  allocated to the  $i$ th subcarrier are increased to

$$P_t(i) = P_t(i) + \Delta P_t(i) \quad (37)$$

$$B(i) = B(i) + \Delta B(i), \quad (38)$$

where  $\Delta B(i) = \log_2(M_{k+1}) - \log_2(M_k)\alpha(i)$ .

After each iteration,  $P_m$  is decreased to

$$P_m = P_m - \sum_j \min(\Delta P_t(j)), \quad 0 \leq j \leq J \leq N - 1, \quad (39)$$

where  $j$  denotes the  $j$ th iteration, and  $J$  stands for the advanced power and bit allocation. The process will be terminated when  $P_m < \Delta P_t(i) = \min(\Delta P_t)$ .

Finally, the expression  $\sum_{i=1}^N \mathbf{B}(i)$  is maximized by implementing the advanced allocation. The order-of-growth of the proposed algorithm is  $(\sum_{i=1}^N \mathbf{B}(i) - K)N \log N$ , where  $K$  is the total number of bit allocated in the primary power and bit allocation process. In the low-SNR regime such as UWB systems, the primary power and bit allocation can significantly lower the total number of algorithm iterations [30].

## VII. SIMULATION RESULTS

In the simulation, a scenario of a point-to-point communication between two cognitive UWB systems is investigated in Matlab. It is assumed that the average number of transmissions per 1ms from the primary users within the communication ranges of the UWB systems follow a Poisson process. In the analysis, the spectral efficiency is used as a performance indicator of the spectral efficiency optimization algorithm. It is derived from normalizing the data rate  $\sum_{i=1}^N \mathbf{B}(i)/T_s$  respect to the operating bandwidth  $W$ .

First, an implementation of the primary and advanced allocation schemes is examined over CM3. Subsequently, the spectral efficiency comparison between the primary and advanced allocation is made under different SNR conditions. Then, the optimized spectral efficiency versus target BER  $\tilde{p}_e$  over different channel models is analyzed. Finally, the optimized spectral efficiency versus the number of the M-QAM zones is discussed. The parameters of the UWB channel model are listed in [5], and the other parameters used to obtain the simulation results are summarized in Table II.

Furthermore, an application with  $T_{txop} = 512 \mu s$  (ACs) is chosen to be activated in the cognitive UWB system. All the results assume a system with a subcarrier spacing of 4.125MHz,  $N=128$  subcarriers, and a Nyquist filter with 0% roll-off and bandwidth 528MHz. The receiver structure employed in this work is based on a coherent detection that assumes perfect channel estimation and no synchronization errors. It is composed of a Discrete Fourier Transform (DFT) demodulator block and parallel to serial converter.

Figure 8 and Figure 9 illustrate the primary and advanced allocation over CM3 with  $\tilde{p}_e = 1e-5$ , respectively. It is observed in Figure 8 that subcarrier-69 is allocated with zero power and bit in primary allocation due to a low corresponding channel gain of -38 dB. During the advanced allocation, as shown in Figure 9,  $P_m$  is iteratively assigned to a subcarrier with the minimum  $\Delta P_t(i)$  to allow the subcarrier to use the higher level of M-QAM modulation. For example, subcarrier-74 is promoted from 8-QAM to 16-QAM by increasing the transmitted power from -48 dB to -42 dB. Each subcarrier is allocated with the maximum possible order M-QAM until the available power  $P_{av}$  is efficiently employed.

Furthermore, the spectral efficiency comparison between the primary and advanced allocation over CM3 with the number of M-QAM levels set to  $M = 4$  is depicted in Figure 10. It is also set  $\tilde{p}_e \in [1e-7, 1e-5]$  and  $SNR_p = \gamma_p$  to -20 dB and -10 dB. The spectral efficiency is significantly improved by at least 25% when the advanced allocation is applied under both  $SNR_p$  conditions. Also, it is observed that the optimized spectral efficiency is improved when the value of  $SNR_p$  is higher. This result is analyzed in Figure 11 in more detail.

It is illustrated in Figure 11 that the values of the optimized spectral efficiency increase exponentially as the estimated  $SNR_p$  value is higher. It is observed that the improvement in spectral efficiency is significant when the  $SNR_p$  increases from -20 to -10 dB over CM3, and is minor when the value

TABLE II  
SIMULATION PARAMETERS

Parameter	Value
$P_{av}$	<-14.1 dBm
$P_f$	0.1
$P_{max}$	-35.1 dBm
$P_d$	0.9
$f_s$	528 MHz
$\gamma_p$	[-20, -18, ..., 0] dB
Subcarrier No.	128
$\tilde{p}_e$	$1e-5 \sim 1e-7$
$W$	4.125 MHz
M-QAM	[2,3,4,8,16]
$T_{txop_i}$	512 $\mu s$
$\lambda$	1/ms

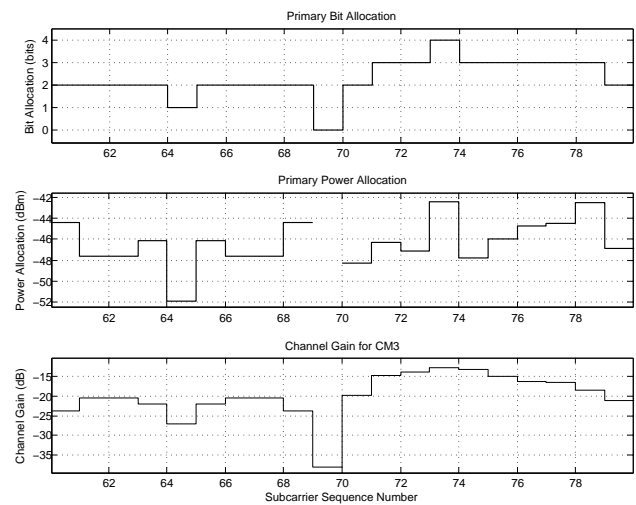


Fig. 8. Primary power and bit allocation

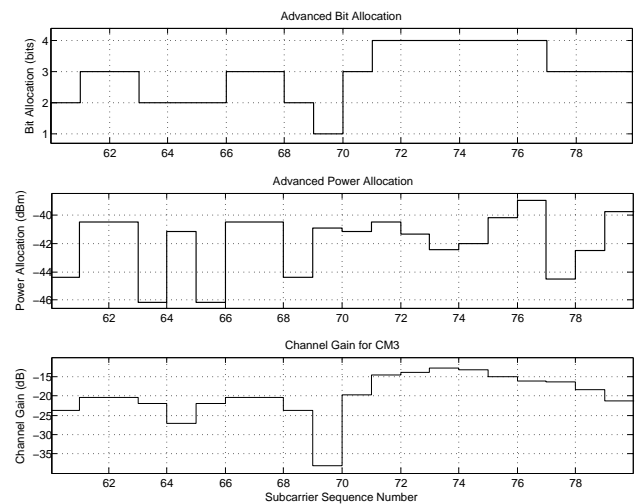


Fig. 9. Advanced power and bit allocation

of  $SNR_p$  increases further. This is due to the fact that the required sensing period  $\tau_s$  decreases exponentially when  $SNR_p$  increase, as expressed in (13).

The choice of the number of M-QAM levels depends on how fast the channel is changing as well as on the hardware

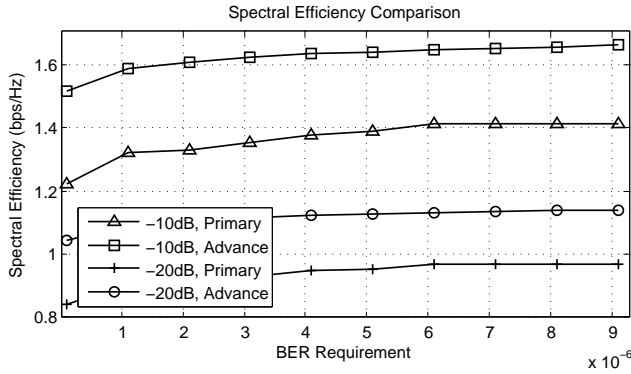


Fig. 10. Primary allocation compared with Advanced allocation, four-point QAM in CM3

constraints [31]. It is shown in Figure 12 that the improvement in spectral efficiency is significant when the number of M-QAM zones increases from 1 to 4 over CM3, and is minor when the number of M-QAM zones increases further. This is due to the fact that the required transmitted power  $P_k(i)$  for a high order M-QAM generally exceeds the maximum allowable transmitted power  $\hat{P}_{max}$  in a subcarrier under the BER requirement  $\tilde{p}_e$ . Thus, to use a large number of M-QAM levels is necessary only when  $\max(P_k(i)) < \hat{P}_{max}$ .

VIII. CONCLUSION AND FUTURE WORK

This paper presents a novel dynamic power and bit allocation scheme for spectral efficiency maximization in the cognitive MB-OFDM UWB radio system. A new BER expression is derived for an in-depth spectral efficiency analysis of UWB multipath channel. The derivation is based on approximating a sum of independent log-normal random variables as another log-normal random variable using the Fenton-Wilkinson method. Then, the performance of the spectral efficiency of the UWB system with equal power allocation is analyzed. This analysis demonstrates the motivation of the design of the dynamic allocation algorithm. To optimize the spectral efficiency and facilitate the convergence of the dynamic allocation algorithm within a small number of iterations, the optimization algorithm is divided into four sections. The results show that the spectral efficiency of the UWB systems is significantly improved when the advanced allocation is applied. The value of the optimized spectral efficiency is significantly improved with the increase of the received  $SNR_p$  value and the number of the M-QAM zones. However, this improvement becomes minor when the  $SNR_p$  value and the number of the M-QAM zones are large.

The uncoded BER expression derived in this work provides a foundation for further study of the coded BER expression with primary user and multiuser interference. More comprehensive analysis of the MB-OFDM UWB time and frequency diversity can be conducted in time variant channel model. Then, a new cognitive power and bit allocation algorithm can be further explored and implemented.

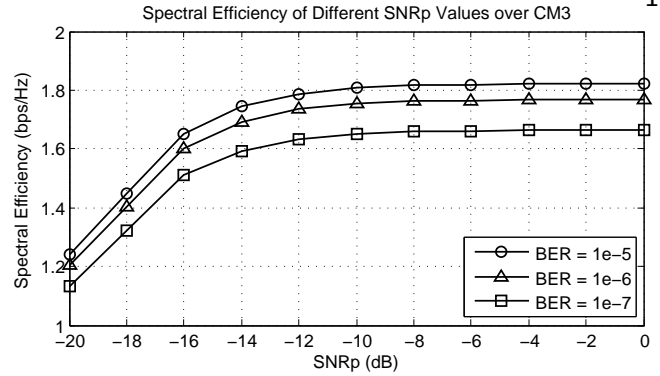


Fig. 11. Optimal Spectral efficiency over CM3 with four-point QAM

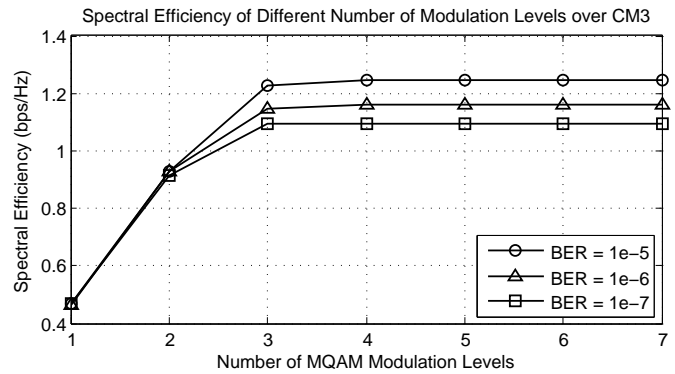


Fig. 12. Optimal Spectral efficiency of different number of modulation levels over CM3,  $SNR_p = -20$  dB

ACKNOWLEDGMENT

The authors wish to thank Michael Barry for his insight and inspiration for the work.

Liaoyuan Zeng’s work on this paper is funded through Irish Research Council for Science, Engineering & Technology (IRCSET) Scholarship.

REFERENCES

- [1] L. Zeng, S. McGrath, and E. Cano, “Rate maximization for Multiband OFDM Ultra Wideband systems using adaptive power and bit loading algorithm,” *Proceedings of the 5th International Conference on Advanced Telecommunications and Systems*, pp. 369–374, May 2009.
- [2] I. J. Mitola and G. Q. Maguire, “Cognitive radio: making software radios more personal,” *IEEE Magazine on Personal Communications*, vol. 6, no. 4, pp. 13–18, Aug. 1999.
- [3] D. Zhang, Z. Tian, and G. Wei, “Spatial capacity of narrowband vs. Ultra-Wideband cognitive radio systems,” *IEEE Transactions on Wireless Communications*, vol. 7, no. 11, pp. 4670–4680, Nov. 2008.
- [4] G. Bansal, M. J. Hossain, and V. K. Bhargava, “Optimal and suboptimal power allocation schemes for OFDM-based cognitive radio systems,” *IEEE Transactions on Wireless Communications*, vol. 7, no. 11, pp. 4710–4718, Nov. 2008.
- [5] A. Batra, J. Balakrishnan, G. Aiello, J. Foerster, and A. Dabak, “Design of a Multiband OFDM system for realistic UWB channel environments,” *IEEE Transactions on Microwave Theory Technology*, vol. 52, no. 9, pp. 2123–2138, September 2004.
- [6] N. Beaulieu, A. Abu-Dayya, and P. McLane, “Estimating the distribution of a sum of independent lognormal random variable,” *IEEE Transactions on Communications*, vol. 43, pp. 2869–2873, December 1995.

- [7] Z. Wang and G. Giannakis, "Wireless multicarrier communications where Fourier meets Shannon," *IEEE Signal Processing Magazine*, vol. 17, no. 3, pp. 29–48, May 2000.
- [8] A. Skelton and S. Fu, "An improved conditional maximum-likelihood detector for noncoherent UWB communication," *IEEE Communications Letters*, vol. 13, no. 1, pp. 7–9, Jan. 2009.
- [9] E. Hossain and V. Bhargava, *Cognitive Wireless Communication Networks*. New York, USA: Springer Science+Business Media, LLC, 2007.
- [10] B. T. Ahmed and M. C. Ramon, "On the impact of Ultra-Wideband (UWB) on macrocell downlink of umts and CDMA-450 systems," *IEEE Transactions on Electromagnetic Compatibility*, vol. 50, no. 2, pp. 406–412, May 2008.
- [11] T. Cormen, C. Leiserson, R. Rivest, and C. Stein, *Introduction to Algorithms*, 2nd ed. Boston, USA: The MIT Press, 2001.
- [12] Y. Chen, G. Yu, Z. Zhang, H. H. Chen, and P. Qiu, "On cognitive radio networks with opportunistic power control strategies in fading channels," *IEEE Transactions on Wireless Communications*, vol. 7, no. 7, pp. 2752–2760, 2008.
- [13] W. Siritwongpairat, W. Su, and K. Liu, "Performance characterization of Multiband UWB communication systems using poisson cluster arriving fading paths," *IEEE Journal on Selected Areas in Communications*, vol. 24, no. 4, pp. 745–751, April 2006.
- [14] H. Lai, W. Siritwongpairat, and K. Liu, "Performance analysis of Multiband OFDM UWB systems with imperfect synchronization and intersymbol interference," *IEEE Journal of Selected Topics in Signal Processing*, vol. 1, no. 3, pp. 521–534, October 2007.
- [15] C. Snow, L. Lampe, and R. Schober, "Performance analysis of Multiband OFDM for UWB communication," *Proceedings of IEEE International Conference on Communications*, pp. 127–130, October 2008.
- [16] "UWB channel modeling contribution from intel," IEEE P802.15-02/279-SG3a., Tech. Rep., 2002.
- [17] S. Ghassemzadeh, R. Jana, C. Rice, W. Turin, and V. Tarokh, "Measurement and modeling of an Ultra-Wide Bandwidth indoor channel," *IEEE Transactions on Communications*, vol. 52, no. 10, pp. 1786–1796, October 2004.
- [18] D. Cassioli, M. Win, and A. Molisch, "The Ultra-Wide Bandwidth indoor channel: From statistical model to simulations," *IEEE Journal on Selected Areas in Communications*, vol. 20, no. 6, pp. 1247–1257, August 2002.
- [19] A. Molisch, "Ultrawideband propagation channels-theory, measurement, and modeling," *IEEE Transactions on Vehicular Technology*, vol. 54, no. 5, pp. 1528–1545, September 2005.
- [20] F. Zheng and T. Kaiser, "On the evaluation of channel capacity of UWB indoor wireless systems," *IEEE Transactions on Signal Processing*, vol. 56, no. 12, pp. 6106–6113, Nov. 2008.
- [21] J. G. Proakis, *Digital Communications*, 4th ed. New York, USA: McGraw-Hill, 2001.
- [22] H. L. V. Trees, *Detection, Estimation, and Modulation Theory*. New York, USA: John Wiley and Sons, 1968.
- [23] Y. Zeng and Y. C. Liang, "Spectrum sensing algorithms for cognitive radio based on statistical covariances," *IEEE Transactions on Vehicular Technology*, vol. 58, no. 4, pp. 1804–1815, May 2009.
- [24] "High rate Ultra Wideband phy and mac standard," ECMA International, Geneva, Tech. Rep., 2005.
- [25] G. L. Stuber, *Principles of Mobile Communication*, 2nd ed. New York, USA: Kluwer Academic Publishers, 2002.
- [26] W. H. Tranter, S. K. Sam, T. S. Rappaport, and K. L. Kosbar, *Principles of Communication Systems Simulation with Wireless Applications*. United States of America: Prentice Hall, 2004.
- [27] A. Goldsmith, *Wireless Communications*. New York, USA: Cambridge University Press, 2005.
- [28] J. Montojo and L. Milstein, "Effects of imperfections on the performance of OFDM systems," *IEEE Transactions on Communications*, vol. 57, no. 7, pp. 2060–2070, July 2009.
- [29] S. Boyd and L. Vandenberghe, *Convex Optimization*. Cambridge, United Kingdom: Cambridge University Press, 2004.
- [30] G. D. J. Forney and G. Ungerboeck, "Modulation and coding for linear Gaussian channels," *IEEE Transactions on Information Theory*, vol. 44, no. 6, pp. 2384–2415, October 1998.
- [31] A. J. Goldsmith and S. G. Chua, "Variable-rate variable-power MQAM for fading channels," *IEEE Transactions on Communications*, vol. 45, no. 10, pp. 1218–1230, Oct. 1997.

# Adaptive MCS Selection with Dynamic and Fixed Sub-channelling for Frequency-Coherent OFDM Channels

Muayad S. Al-Janabi, Charalampos C. Tsimenidis, *Member, IEEE*, Bayan S. Sharif, *Senior Member, IEEE* and Stéphane Y. Le Goff School of Electrical, Electronics and Computer Engineering  
Newcastle University, Merz Court, NE1 7RU, Newcastle upon Tyne, UK

**Abstract**—This paper presents two strategies for joint adaptive modulation and coding (AMC) techniques. The first strategy is based on the fixed sub-channel (FS)-AMC allocation, which exploits the coherence bandwidth of the wireless channel to divide the transmitted frame into independent sub-channels that correspond to the channel coherence bandwidth as well as selecting the optimal modulation and coding scheme (MCS) for each individually. The second strategy is based on dynamic sub-channel (DS)-AMC allocation, reduces the size of pilot sub-carriers for the stable sub-channel profiles; where the redundant pilots are replaced with additional data sub-carriers, which enhance the total system throughput. These strategies are implemented for orthogonal frequency division multiplexing (OFDM) systems with channel state information (CSI) feedback. Low density parity check (LDPC) codes are utilized for encoding by employing signal-to noise ratio (SNR) dependent coding rates, as well as distinct modulation schemes to achieve adaptivity to time-varying channel conditions. The performance of the proposed system was tested on Rayleigh fading channels that exhibit frequency coherent bands. Numerical results obtained via simulation demonstrate that the throughput and bit error rate (BER) performances of both proposed systems are better than previously suggested approaches. Additionally, there is a significant improvement in the throughput performance of the dynamic sub-channel allocation strategy over the fixed sub-channel allocation method.

**Index Terms**—Frequency channel coherent, sub-channelling, OFDM, AMC, MCS.

## I. INTRODUCTION

Recently, the requirements for achieving high performance in wireless communications systems have increased dramatically. These requirements have focused on the schemes that increase the transmission of data as well as minimizing the BER at the receiver. OFDM for single user and orthogonal frequency division multiple access (OFDMA) for multiuser are examples of such powerful systems. The above two systems have been adopted by many standards including Fixed WiMAX IEEE 802.16 and Mobile WiMAX IEEE 802.16e. They demonstrate high ability to tackle the degradations introduced by multipath channels that cause inter symbol interference (ISI) at low computational complexities. However, the transmitted waveforms of these systems exhibit high peak-to-average power ratio (PAPR) and are sensitive to Doppler shifts, which produce inter carrier interference (ICI) [1]-[8].

OFDM and OFDMA systems are implemented in practice using error correcting schemes, such as convolutional, turbo

and LDPC codes. In this paper, we adopt LDPC codes since they exhibit lower computational complexity. LDPC codes were invented by Gallager in 1963 as a class of linear codes. Their main feature is a sparse generator matrix which comprises a low density of ones. Nowadays, LDPC codes are widely employed in AMC strategies to select suitable modulation and coding rates for OFDM and OFDMA sub-carriers based on returned CSI. The aim is to avoid the additional iterative processing, which is impractical with real-time systems, since LDPC decoding already incorporates iterations inside its decoder [9]-[11].

Most research studies so far have focused on AMC for OFDM systems without any consideration of the frequency coherence of the underlying wireless channel. In [12], AMC for OFDM schemes was presented, which divided the OFDM frame into fixed clusters, with each cluster exhibiting independent modulation and coding schemes according to CSI that was returned from the receiver. In [13] and [14], the implementation of adaptive bit-interleaved coded modulation (BICM) with OFDM was introduced depending on the returned CSI obtained from the estimated BER. However, they considered the OFDM frame as a one part with same MCS for all symbols. In [15], a novel two-step channel prediction technique has been proposed that considered the time-varying nature of a channel over the duration of interest that produced the required CSI to the transmitter to achieve adaptivity.

Reliable transmission of the information stream was ensured by utilising the lowest and fixed MCS levels in [16]. Moreover, this method was also very efficient for a large number of sharing users per transmitted frame. To increase the system performance, two strategies were used; the first strategy enhanced the system throughput by employing the AMC technique to exploit the capacity of the channel; the second strategy adopted the link-layer auto repeat request (LARQ) and hybrid auto repeat request (HARQ) to increase the transmitted packet error rate and to reduce the convolutional code gain in order to detect the error of the received data packet.

In [17], the AMC technique was used in a wideband code division multiple access (WCDMA) downlink to enhance the scheduling performance; at the same time, a fast cell selection (FCS) strategy was adopted. In this work, the Round Robin (RR), the simplified proportional fair (PF), the maximum carrier to interference ratio(C/I), and the conventional PF schemes were investigated and compared as scheduling techniques.

Moreover, the authors tried to maximise the user throughput in a cellular network by proposing an optimal selection of the MCS options. The system was based on the Chase Combining and Incremental Redundancy schemes for the HARQ mechanism. The optimal MCS selection was dependent on the number of transmissions and successful decoding probability in the HARQ operation.

The authors of [18] adopted the SNR-based and buffer-assisted AMC technique strategies of selection to analyse the channel packet transmission and re-transmission system. In this work, the size and status of the transmit buffers have been considered during the design and analysis of the performance, efficiency, and complexity measurements.

The impact for the estimated channel errors in a CDMA system, which used the AMC strategy with multi-codes, was presented in [19]. Moreover, the communication channel was modelled utilising Simple Moving Average (SMA) and Hidden Markov Model (HMM) filters. In [20], a link adaptation algorithm with Packet Error Rate (PER) was presented. The PER performance was predicted for the coded multiple-antenna OFDM system based on the detected error of the channel estimation.

In [21], a comparison of the throughput performance between Single-Carrier transmission with Frequency-Domain Equalisation (SCFDE) and OFDM over the non-linear fading channels was presented. The transmitted power was used as a metric with the AMC criteria to overcome the transmission drawbacks. On the other hand, an efficient Medium Access Control (MAC) technique based on AMC strategy was presented in [22]. The packet format was varied based on the channel state to achieve a high performance system and an optimal analytical model was proposed for the non-stationary transmission link. In addition, a comparison between the analytical evaluations and simulation results was presented to show the outperformance of the proposed system. Additionally, in [23], a cross-layer design over the data link and physical layer was derived, the optimal system performance was achieved by exploiting the truncated ARQ protocol ability to correct the transmission errors as well as the using AMC strategy features.

Issues concerning the distribution methods of the pilot along the OFDM frame have been widely addressed in recent research work. The two main prevailing approaches are the block and comb pilot distribution methods [24]-[26].

The first key contribution of our paper is to produce an FS-AMC-OFDM scheme that exploits the frequency coherence of the channel by dividing the OFDM frame into sub-channels that correspond to the detected channel coherence bands at the receiver. Subsequently, each individual sub-channel is assigned its own independent MCS. The second contribution is to present a DS-AMC-OFDM system, which reduces the number of pilot sub-carriers within the individual stable profile sub-channels and replaces the unused sub-carriers by additional information streams. This reduction is dependent on the SNR fluctuation values of the sub-channels, and the sub-channels' minimum SNR values. Moreover, in order to achieve an optimum channel estimate, pilots are inserted and interleaved across the frame data using the comb method [24]-[25]. The

proposed AMC strategy is established on six adapting options that support the flexibility of switching between MCS schemes in real time to reach the required performance.

The remainder of the paper is organized as follows. In Section II, the description of the proposed system is presented. Section III outlines the LDPC decoding algorithm, while the proposed transmission techniques is introduced in Section IV. Section V demonstrates the performance of the proposed systems via simulation results. Finally, conclusions are drawn in Section VI.

## II. SYSTEM MODEL DESCRIPTION

This section outlines the proposed FS-AMC-OFDM and DS-AMC-OFDM systems. In these schemes, LDPC codes are considered with three different coding rates in conjunction with two modulation schemes, i.e. 16 quadrature amplitude modulation (16-QAM) and quadrature phase shift keying (QPSK) modulation. These two modulation types combined with three coding rates produce six individual MCSs.

The transmitted OFDM frame of the proposed system contains  $N$  sub-carriers, which are divided into  $N_p$  pilots,  $N_d$  data, and  $N_G$  guard sub-carriers. The pilots are distributed uniformly into groups corresponding to the number of detected frequency coherence bands  $N_{\text{coh}}$  of the channel.

For the FS-AMC-OFDM system, each sub-channel adopts a distinct MCS and contains  $\alpha_d(i) = N_d/N_{\text{coh}}$  data and  $\alpha_p(i) = N_p/N_{\text{coh}}$  pilot sub-carriers, where  $i = \{1, \dots, N_{\text{coh}}\}$  is the index of the sub-channels. The number of the selected MCS for each group of symbols is sent to the transmitter via the returned CSI, instead of estimating the channel and SNR values in order to reduce the size of the feedback information required. On the other hand, the size of data  $\alpha_d(i)$  and pilot  $\alpha_p(i)$  sub-carriers, within sub-channels can be changed for DS-AMC-OFDM system according to the returned channel conditions. The CSI is assumed to be returned using time division duplex (TDD) link without any feedback delay due to the short transmission distance.

The proposed systems are applicable in many transmission environments and they require identical implementation complexity to the related conventional AMC based transmission schemes that utilize same MCSs. The proposed systems are described in detail in the following sub-sections.

### A. FS-AMC-OFDM system

The investigated FS-AMC-OFDM system can be divided into the following three parts.

*1. Transmitter:* The transmitter comprises three main blocks as shown in Fig. 1. The first block generates, from the binary data, different coded and modulated symbol groups that are assigned to different sub-channels. The second block assembles the OFDM signalling frame from the modulated data and the pilots, which are inserted at uniform positions using a comb approach. The final part of the transmitter implements the inverse fast Fourier transform (IFFT) and CP

insertion operations. The transmitted OFDM frame can be mathematically represented as:

$$x(k) = \frac{1}{\sqrt{N_{\text{FFT}}}} \sum_{n=1}^{N_{\text{FFT}}} X(n) e^{j \frac{2\pi k n}{N_{\text{FFT}}}}, \quad (1)$$

where  $x(k)$  are the transmitted OFDM waveform samples in time-domain,  $X(n)$  denotes the OFDM symbols assigned to each data sub-carrier,  $N_{\text{FFT}}$  is the FFT size and  $k = \{1, \dots, N_{\text{FFT}}\}$  and  $n = \{1, \dots, N_{\text{FFT}}\}$  are the time and frequency domain indices, respectively.

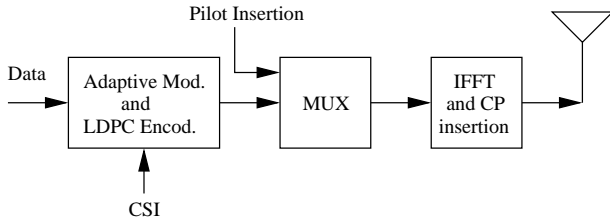


Fig. 1. Transmitter block diagram of the proposed FS-AMC-OFDM system.

**2. Channel Model:** It is known that there are many types of coherent channels, such as time variant and invariant channels for both fast and slow fading. The frequency response of these channels can be more or less selective in terms of the selected sub-carriers. This selectivity may decrease the coherence bandwidth, which in turn increases the utilized sub-channels in our proposed system.

In this paper, a wireless Rayleigh fading communication channel is considered in this paper. A key assumption is that the channel exhibits coherence frequency bands, thus, the total system bandwidth is divided into sub-channels that are time-varying but flat in terms of attenuation for all sub-carriers within the same band. The individual sub-channel values are assumed to be correlated between subsequent symbols. The impulse response of the channel is given as:

$$h(k) = \sum_{l=0}^{L-1} h_l(k) \delta(\tau_l), \quad (2)$$

where  $L$  is the number of taps,  $\tau_l$  is the time delay associated with the  $l$ -th tap and  $h_l(k)$  is the complex-valued channel fading coefficient of the  $l$ -th tap for the time index  $k$ . The coherence bandwidth  $B_{\text{coh}}$ , which represents the frequency correlation between channel gains, is given for values above 0.9 as:

$$B_{\text{coh}} = \frac{1}{50\sigma_\tau}, \quad (3)$$

where  $\sigma_\tau$  is the root mean square (rms) of the multipath delay spread in the time domain, given as:

$$\sigma_\tau = \sqrt{\frac{\sum_{l=0}^{L-1} |h_l(k)|^2 \tau_l}{\sum_{l=0}^{L-1} |h_l(\tau_l)|^2}}. \quad (4)$$

Fig. 2 demonstrates an example of the system channel with 20 MHz bandwidth suited to propagate one OFDM frame. This model is based on the Rayleigh channel properties and exhibits

15 taps. In this figure, part (a) represents the the channel time impulse response, while (b) is the channel frequency response in dB.

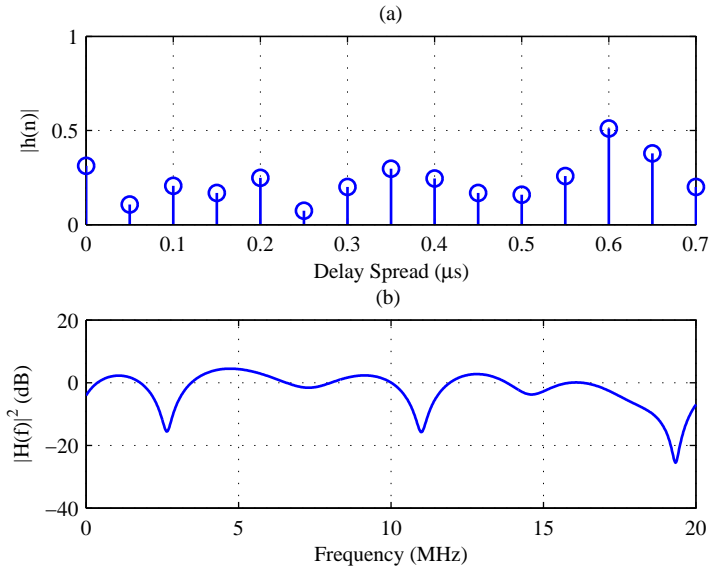


Fig. 2. Channel model.

**3. Receiver Description:** The receiver structure is illustrated in Fig. 3. After the cyclic prefix has been removed, the received OFDM frame can be represented as:

$$y(k) = r(k) + w(k) = x(k) \otimes h(k) + w(k), \quad (5)$$

where  $y(k)$  are the received samples,  $h(k)$  refers to the channel coefficients,  $w(k)$  represents the additive white Gaussian noise (AWGN) samples,  $\otimes$  denotes the circular convolution operation. The result of the circular convolution,  $r(k)$ , between the transmitted OFDM samples and the channel values is defined as:

$$r(k) = \sum_{l=0}^{L-1} h(l) x((k-l))_N, \quad k = 0, \dots, N-1. \quad (6)$$

After the FFT operation is applied to the entire OFDM frame, the received signal samples can be expressed as:

$$Y(n) = X(n)H(n) + W(n). \quad (7)$$

Following the FFT operation, the pilots and the data are extracted from the received OFDM frame. The pilots are utilized in the channel estimation algorithm and CSI unit, which produces the estimated channel and SNR values, as well as, the decision of suitable MCS for each sub-channel. Finally, the data are demodulated and decoded in the same selected transmitted MCSs. In this paper, a Mobile WiMAX IEEE 802.16e system is considered with the parameters listed in Table I. The performance of the investigated FS-AMC-OFDM system is effected by many utilized parameters, such as the data and pilot sub-carriers number as well as the employed bandwidth.

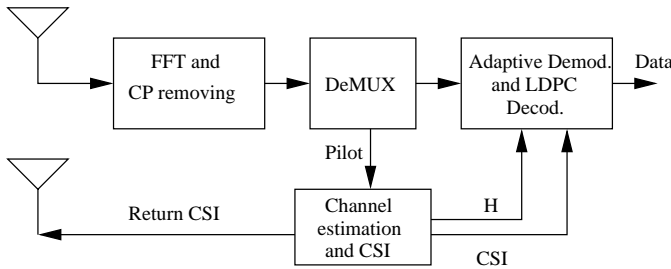


Fig. 3. Receiver block diagram of the proposed FS-AMC-OFDM system.

TABLE I  
SYSTEM PARAMETERS

No	Parameter	Value
1	Bandwidth	20 MHz
2	Number of FFT	2048
3	Number of data carrier	1440
4	Number of pilot carrier	240
5	Number of guard sub-carrier	368
6	Cyclic prefix	1/4
7	Coherence bandwidth	4 MHz

*B. DS-AMC-OFDM system*

This section considers the developments applied to the FS-AMC-OFDM system structure in order to produce an efficient scheme, which uses dynamic allocation for the data and pilot sub-carriers across the distinct sub-channels instead of a fixed allocation strategy. The transmitter block diagram of the proposed DS-AMC-OFDM system is similar to FS-AMC-OFDM, where the first block (Adaptive Mod. and LDPC Encod.) decides the size of the transmitted information bit stream for each sub-channel according to the returned CSI. At the same time, the pilot generator can reduce or increase the pilot stream size for each coherence bands based on the corresponding returned pilot size.

The selectivity of the utilized channel frequency response can effect the performance of the DS-AMC-OFDM system particularly for the narrow coherence bandwidth channels. For these channels, the proposed system uses all the employed pilots for channel estimation. We use the same channel model of the FS-AMC-OFDM system, while the receiver adds another block to adjust the size of the data and pilot symbols for each sub-channel individually as explained in the next section.

*1. Receiver:* Fig. 4 illustrates the DS-AMC-OFDM system receiver. From this figure, the size of the pilot and data for each sub-channel is adjusted in the additional, Size Adjustment, block. The main function of the new block is to decide a suitable size for the data and pilot across the sub-channels individually, while the other receiver's blocks have the same functions of the FS-AMC-OFDM system receiver. For stable channel conditions, the pilots' size is reduced and the available size from this reduction is filled with additional data symbols at the transmitter to increase the total transmission throughput. The selected sizes of the pilots of each sub-channel is included

in the returned CSI.

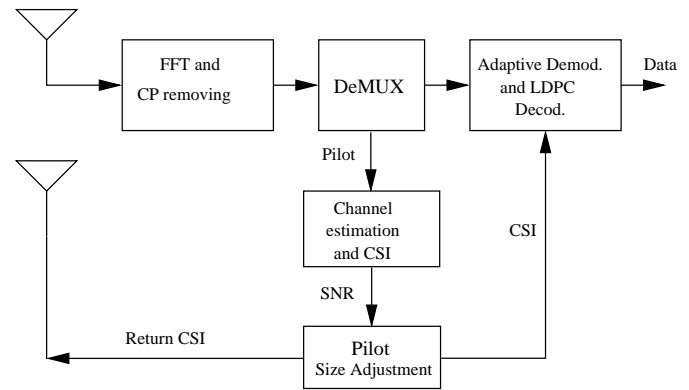


Fig. 4. Receiver block diagram of the proposed DS-AMC-OFDM system.

III. LDPC DECODING

As the proposed systems follow the Mobile WiMAX standard, we employ LDPC as one of the recommended error correction methods. The LDPC codes that have been adopted in this paper are irregular repeat accumulate codes which have a high ability to detect and correct the receiving errors depending on the error probability density function (pdf). The LDPC encoding and decoding processes are explained as follows.

*A. LDPC encoder*

LDPC encoding is performed by generating a parity check matrix, which must be a sparse matrix with a specified number of columns and rows according to the codeword size and employed code rate respectively. To obtain the encoded data sequence, the entire binary data vector is multiplied by a generator matrix, which is derived from the parity check matrix [27]. Fig. 5 shows the LDPC encoding process block diagram.

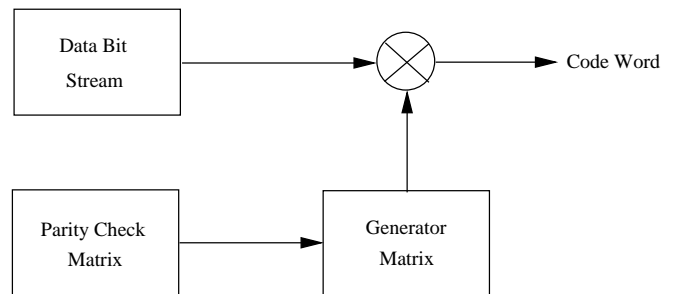


Fig. 5. LDPC encoder block diagram.

*B. LDPC decoder*

The algorithms performing the LDPC decoding process produce efficient and iterative methods to decode the received data bits. In this paper the message passed algorithm

is adopted. This algorithm is also known as the belief propagation algorithm, and sum-product algorithm. The message passed algorithm is based on decoding the coded bits in iterative manner as a message between the bit and check nodes shown in Fig. 6 illustrating the Tanner graph. It is implemented using four processing steps, i.e. initialization, check node update, bit node update and hard decision. We now proceed with the description of the individual steps [27].

1. *Initialization:* Set the loop iteration,  $l = 0$ ,

$$\eta_{m,n}^{[0]} = 0, \quad \forall (m, n) \text{ with } A(m, n) = 1, \quad (8)$$

$$\lambda_n^{[0]} = L_c r_n. \quad (9)$$

where  $\mathbf{A}$  is the parity check matrix,  $L_c$  is the channel reliability,  $\lambda$  and  $\eta$  are the messages from bit nodes to check nodes, and check to bit nodes, respectively.

2. *Check node update:*

$$l = l + 1. \quad (10)$$

$$\eta_{m,n}^{[l]} = -2 \tanh^{-1} \left( \prod_{j \in N_{m,n}} \tanh \left( -\frac{\lambda_j^{[l-1]} - \eta_{m,j}^{[l-1]}}{2} \right) \right). \quad (11)$$

3. *Bit node update:*

$$\lambda_n^l = L_c r_n + \sum_{m \in M_n} \eta_{m,n}^{[l]}. \quad (12)$$

4. *Hard decision:*

$$c_n = \begin{cases} 1, & \text{if } \lambda_n > 0 \\ 0, & \text{otherwise} \end{cases} \quad (13)$$

if  $(\mathbf{A}\mathbf{c}' = 0)$ , then stop;  
 else if  $(l < L)$  go to check node update;  
 otherwise exit;  
 Here,  $c_n$  are the decoded data bits,  $L$  is the maximum number of iterations, and  $\mathbf{c}'$  is the vector containing the decoded bits at the end of the final iteration.

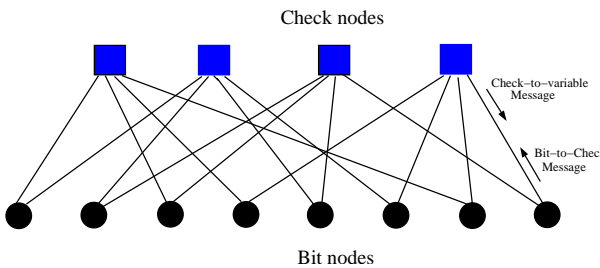


Fig. 6. LDPC decoding algorithm Tanner graph.

#### IV. PROPOSED AMC-LDPC-OFDM TRANSMISSION TECHNIQUES

The LDPC encoder encodes the entire data sequence using one of the three possible code rates (1/2, 2/3 or 3/4). Furthermore, two modulation schemes are available for sub-channels in order to satisfy their selected MCSs, i.e. QPSK and 16-QAM. In this section, the proposed transmission strategies of both systems are described separately.

#### A. FS-AMC-OFDM strategy

The novelty of this system is the introduction of distinct MCSs that correspond to the detected frequency coherent sub-channels. The  $N_p$  pilots are modulated using BPSK to guarantee insensitivity to channel effects at both low and high SNR levels. Additionally, they are distributed across the data symbols according to the comb-method by allocating one pilot carrier for every six data symbols, as illustrated in Fig. 7.

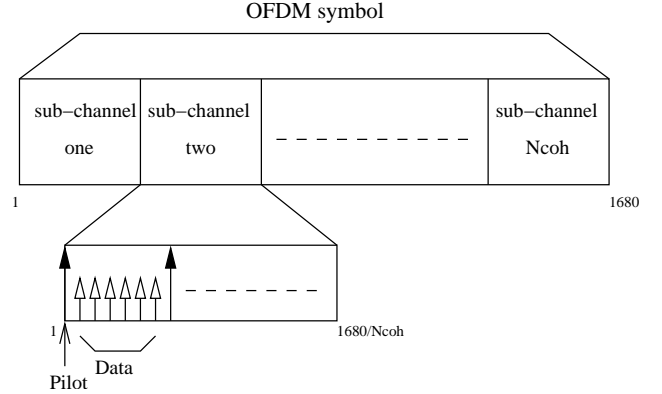


Fig. 7. AMC-LDPC-OFDM transmitted block frame.

At the receiver, channel and SNR estimation, as well as the decision on MCS selection for each sub-channel are performed. The channel estimation was implemented using the least square (LS) method [28]:

$$\hat{H}_p(i, m) = D[X_p(i, m)]^{-1} Y_p(i, m), \quad m = 0 \dots \alpha_p(i) - 1, \quad (14)$$

where  $\hat{H}_p(i, m)$  are the estimated pilot channel values,  $D[X_p(i, m)]$  is a diagonal matrix constructed using the known transmitted pilot symbols, and  $Y_p(i, m)$  are the received pilot symbols after the FFT operation. In this paper, the channel estimation error is not considered. It is caused by imperfect synchronization, feedback delay and channel estimation. The channel estimation error can be added as a noise to the received signal as  $Y(n) = X(n)\hat{H}(n) + X(n)[H(n) - \hat{H}(n)] + W(n)$ . Furthermore, the channel estimation error effects the computed value of the corresponding SNR, where  $\hat{H}(n)$  denotes the estimated channel coefficients. The channel values that relevant to the data sub-carrier are obtained by averaging neighbour pilots instead of using interpolation methods to reduce the complexity. A two-sample average was utilized based on the assumption that the channel will remain constant throughout the duration of an OFDM block, i.e.

$$\hat{H}_d(i, z) = \frac{1}{2} \left[ \hat{H}_p(i, m) + \hat{H}_p(i, m + 1) \right], \quad (15)$$

$$m = \text{mod}(z, N_p), \quad z = 0 \dots (\alpha_d(i)/\alpha_p(i)) - 1, \quad (16)$$

where  $\hat{H}_d(i, z)$  represents the  $z$ -th data sub-carriers between two pilots for each sub-channel, and  $m$  denotes the index of corresponding pilot.

Furthermore, the SNR is estimated for each symbol in the OFDM frame and the minimum value for each sub-channel

$\gamma_{i,\min}$  is selected to guarantee that the required performance is maintained:

$$SNR_d(i, v) = \frac{E\{|\hat{H}_d(i, v)|^2 |X(i, v)|^2\}}{E\{|W(i, v)|^2\}} \quad (17)$$

$$= \frac{E\{|\hat{H}_d(i, v)|^2\} E\{|X(i, v)|^2\}}{E\{|W(i, v)|^2\}} \quad (18)$$

$$= E_s \frac{E\{|\hat{H}_d(i, v)|^2\}}{\sigma_W^2(i, v)} \quad (19)$$

where  $\sigma_W^2(i, v)$  is the AWGN variance,  $E_s = E\{|X(i, v)|^2\}$  is the average sub-channel symbol energy, which is 1 for QPSK and  $10d^2$  for 16-QAM, where  $d$  is the minimum distance between constellation points. In practice, we can replace  $E\{|\hat{H}_d(i, v)|^2\}$  with the estimated channel values  $|\hat{H}_d(i, v)|^2$ , where  $v = \{1, \dots, \alpha_d(i)\}$  is the sub-channel data symbols index. The minimum SNR is then obtained as:

$$\gamma_{i,\min} = \min[SNR_d(i, v)] = \min \left\{ E_s \frac{|\hat{H}_d(i, v)|^2}{\sigma_W^2(i, v)} \right\} \quad (20)$$

The selection of suitable MCS for each sub-channel is based on the estimated SNR of the corresponding sub-channel according to Table II, which considers the threshold SNR values for a BER of  $10^{-3}$  [12]. The diversity of MCSs

TABLE II  
SNR THRESHOLD VALUES FOR MCS

Modulation type	Code rate	Threshold dB
QPSK	1/2	4.5
QPSK	2/3	5.6
QPSK	3/4	8.2
16-QAM	1/2	10.5
16-QAM	2/3	11.9
16-QAM	3/4	> 11.9

for symbol groups that are included in the same OFDM frame improves the system throughput  $\mu$  by increasing the transmitted throughput  $\psi_{av}(i)$ , which depends on the sub-channel symbol coding rate  $R_c(i)$  and the modulation order  $M(i)$ , and is given as [12]:

$$\psi(i, v) = \log_2[M(i)]R_c(i). \quad (21)$$

In terms of the probability of the MCS selection, the system throughput can be mathematically expressed as:

$$\mu = \sum_{i=1}^{N_{MCS}} P_r\{MCS(i)\} \psi_{av}(i) (1 - SER), \quad (22)$$

where  $P_r\{MCS(i)\}$  denotes the probability of choosing each MCS,  $\psi_{av}(i) = E\{\psi(i, n)\}$  is the average transmitted throughput in bit/symbol,  $SER$  is symbol error rate and  $N_{MCS}$  is the number of MCSs. Additionally, the decrease of  $SER$ , which depends on selection of the optimum MCS for the channel type ( $P_r\{MCS(i)\}$ ), leads to an increase in the system throughput as shown in Eq. (22).

On the other hand, the system throughput can be expressed in terms of the size of the transmitted data of each sub-channel,  $\alpha_d(i)$ , the average transmitted throughput,  $\psi_{av}(i)$ , and the average sub-channel bit error rate,  $P_e(i)$ , as follows:

$$\mu = \sum_{i=1}^{N_{coh}} \alpha_d(i) \psi_{av}(i) [1 - P_e(i)]. \quad (23)$$

From Eq. (23), the throughput, which is the successful received bits, is based mainly on the size of the transmitted data symbols. This leads to the ability of enhancing the proposed system throughput performance by increasing the transmitted data size as explained in the next section.

### B. DS-AMC-OFDM strategy

The proposed DS-AMC-OFDM system exploits the scalability of OFDM systems such as Mobile WiMAX, which endorses the reduction in pilots, to improve the throughput by replacing the unnecessary pilots within a channel coherence band with information data streams; and hence increase the total transmitted throughput. This reduction in the number of pilots for each sub-channel individually depends on the variance of the sub-channel SNR fluctuation values,  $\Gamma_{var}(i)$ , and the sub-channel  $\gamma_{i,\min}$ . The range of the pilot reduction  $\lambda(i)$  can be varied between zero and  $\alpha_p - 2$ .

To measure the coherence bandwidth, which is required to obtain the number of the sub-channels, a correlation process between the channel coefficients is adopted in the frequency domain. It assumes that the correlation between the channel coefficients frequency response depends only on the  $B_{coh}$ . The correlation value of the channel can be achieved as:

$$\beta_{B_{coh}} = \frac{E\{[\hat{H}(f) - \eta_{\hat{H}(f)}][\hat{H}(f)(f + B_{coh}) - \eta_{\hat{H}(f+B_{coh})}]^*\}}{E\{|\hat{H}(f)|^2\}} \quad (24)$$

where,  $\eta_{\hat{H}(f)}$  and  $\eta_{\hat{H}(f+B_{coh})}$  are the mean values of the channel frequency responses, and  $f$  is the frequency index. The uniform distribution of the phase of the Rayleigh channels leads to  $\eta_{\hat{H}(f)}$  and  $\eta_{\hat{H}(f+B_{coh})}$  values to be zero, thus Eq. (24) can be rewritten as:

$$\begin{aligned} \beta_{B_{coh}} &= \frac{E\{[\hat{H}(f)][\hat{H}(f)(f + B_{coh})]^*\}}{E\{|\hat{H}(f)|^2\}} \\ &= \frac{E\{[\hat{H}(f)][\hat{H}(f)(f + B_{coh})]^*\}}{\sigma_{\hat{H}(f)}^2}, \end{aligned} \quad (25)$$

where  $\sigma_{\hat{H}(f)}^2$  is the channel variance. By varying the  $B_{coh}$ , which is the correlation lag, in an iterative method and keeping the correlation value over 0.9, we can obtain the coherence bandwidth, where the channel responses for frequencies separated by  $B_{coh}$  or less, are nearly equal. As a result,  $N_{coh}$  is calculated based on the total system bandwidth (BW) as  $N_{coh} = \frac{BW}{B_{coh}}$ .

The SNR fluctuation of the channel coefficients within each coherence band is evaluated depending on the estimated SNR values as:

$$\Gamma(i, n) = SNR_d(i, v) - \varrho(i), \quad (26)$$

where  $\varrho(i) = E\{SNR(i, v)\}$  is the average SNR value for each sub-channel. The  $\Gamma_{var}(i)$  value can be calculated as:

$$\Gamma_{var}(i) = E\{|\Gamma(i, n)|^2\}. \quad (27)$$

Based on the detected coherence bandwidth, the number of pilots and data for each sub-channel is set. Moreover, the number of required pilots for the channel estimation is mainly dependent on the fluctuation values between the neighbouring pilots. The SNR values of each sub-channel  $\gamma_{i,min}$  are further used to measure the stability of the channel state in terms of the noise. The equations describing the dynamic adjustment of pilots and data streams can be written as:

$$\vartheta_p(i) = \alpha_p(i) - \lambda(i), \quad (28)$$

$$\vartheta_d(i) = \alpha_d(i) - \lambda(i), \quad (29)$$

$$\lambda(i) = \xi(i) \frac{\gamma_{i,min}}{\Gamma_{var}(i)}, \quad (30)$$

where  $\vartheta_p(i)$  and  $\vartheta_d(i)$  designate the new number of pilots and data for each sub-channel, respectively, and  $\xi(i)$  is a variable chosen to satisfy the condition,  $\text{mod}[\vartheta_d(i)/\vartheta_p(i)] = 0$ , that guarantees a uniform distribution of pilots and data within each sub-channel. The size of the pilot subcarriers of each sub-channel is included in the CSI to permit the transmitter to adjust the transmission sizes. The resulting system throughput,  $\mu$ , in Eq. (23) can be mathematically rewritten as:

$$\mu = \sum_{i=1}^{N_{coh}} \vartheta_d(i) \rho_{av}(i) [1 - P_e(i)]. \quad (31)$$

Evidently, the increase in the transmitted data stream size is expected to increase the system throughput performance. At the same time, the optimal selection of the suitable MCS for the sub-channels can decrease the BER, which leads to increase the throughput. To measure the effect of the pilot reduction on the channel estimation process, the mean square error (MSE) of the estimated channel value in comparison with the perfect channel  $H(i, n)$  and is calculated as:

$$MSE(i) = E\{|\hat{H}(i, n) - H(i, n)|^2\} \quad (32)$$

and the total MSE is evaluated as  $TMSE = E\{MSE(i)\}$ .

## V. SIMULATION RESULTS

The performance of the proposed FS-AMC-OFDM and DS-AMC-OFDM systems are investigated in Rayleigh fading channels exhibiting five frequency coherence bands. The parameters of the Mobile WiMAX standard listed in Table I have been utilized for the simulation. The performance of the investigated systems depends on the utilized parameters for each transmitted OFDM frame. However, both systems still outperform the conventional scheme for the same considered parameters as shown in the next sub-sections. The simulation results of the proposed systems are divided into two parts as follows.

### A. FS-AMC-OFDM system

This section demonstrates and discusses the simulation performance of FS-AMC-OFDM system. Fig. 8 shows the throughput comparison between two systems; a conventional adaptive system which adopts the same MCS for the whole OFDM frame, and the proposed adaptive system. It is observed that the proposed scheme provides a throughput related performance gain between 0.1-1.2 Mbit over the conventional adaptive system for a SNR range between 5 and 35 dB. The enhancement in performance is due to the fact that the proposed strategy exploits the channel conditions to construct the transmitted OFDM frame, which contains different types of modulation and coding rates that are related to the coherence bandwidth of the underlying channel. Moreover, the suggested approach benefits from the fading diversity on sub-channels to increase the transmitted throughput, which in turn improves system performance by increasing the coding rate and modulation level as indicated in Eq. (21) and (22). It is worth observing that at high SNR levels above 35 dB the performance of the adaptive systems approximately converges to the same value because they select the same MCS for all sub-channels.

Fig. 9 demonstrates the difference in transmitted throughput between the conventional adaptive and proposed approaches. It is apparent that the performance of proposed system achieves 0.1-0.6 bit/symbol better than the conventional over a SNR range between 5 and 35 dB.

Fig. 10 illustrates the average BER performance as a function of the SNR for the two investigated systems. After 10 dB of SNR, the plot shows clearly the performance advantage of the proposed adaptive scheme. The improvement is due to the optimal MCS selection for each sub-channel, which in turn, enhances the BER performance. However, for high SNR values, the difference in performance between the two adaptive schemes is approximately the same, since their constructed transmitted OFDM frames become nearly identical.

Fig. 11 displays the behaviour of the proposed AMC-LDPC based OFDM system in terms of selecting the maximum reliable data size, which is computed by averaging each

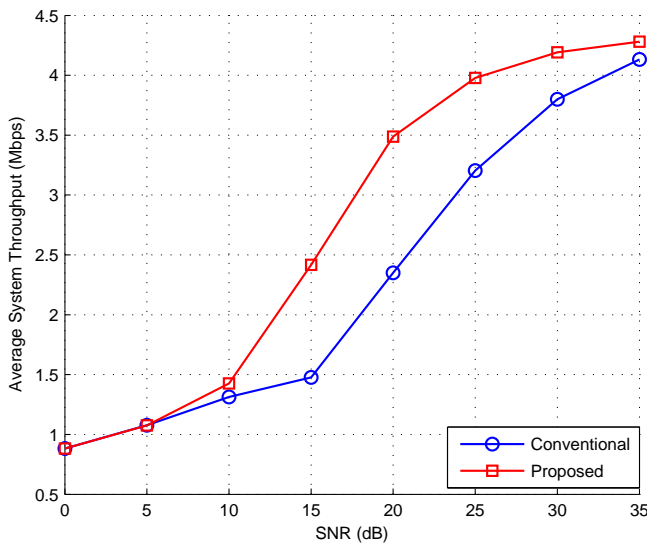


Fig. 8. Throughput of the conventional and proposed FS-AMC-OFDM system.

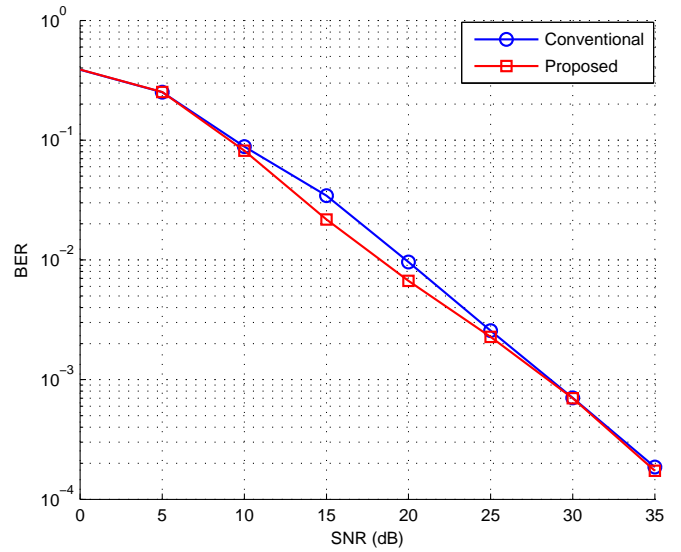


Fig. 10. BER of the conventional and proposed FS-AMC-OFDM system.

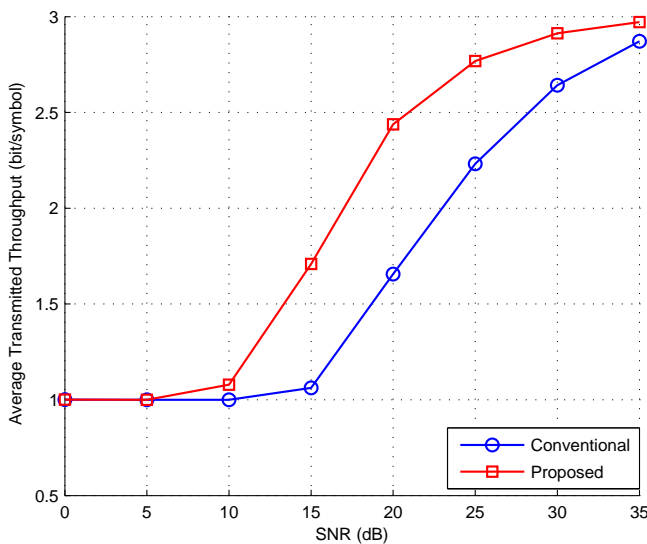


Fig. 9. Transmitted throughput of the conventional and proposed FS-AMC-OFDM system.

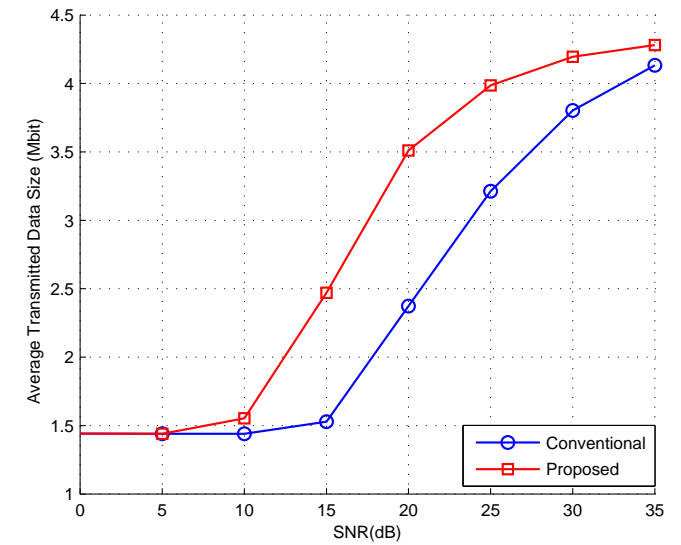


Fig. 11. Transmitted data size of the conventional and proposed FS-AMC-OFDM system.

sub-channel. It should be highlighted that individual points in this graph may contain different types of coding rates and modulation levels. From the diagram, it is apparent that the proposed scheme outperforms the conventional adaptive system. Moreover, it should be noted that at 35 dB of SNR, the data size is chosen to be maximum, indicating that all sub-channels have same modulation type (16-QAM) and coding rate ( $R=3/4$ ).

### B. DS-AMC-OFDM system

The simulation results related to the performance of the DS-AMC-OFDM system are presented in this section. The

size of the pilot and data sub-carriers for each sub-channel are adjusted the distinct criteria listed in Table III.

Fig. 12 demonstrates the throughput performance of the conventional, the proposed FS-AMC-OFDM, and the proposed DS-AMC-OFDM systems. It is important to notice that the throughput of proposed DS-AMC-OFDM system outperforms the FS-AMC-OFDM scheme by 0.1-0.7 Mbps over an SNR range of between 5 and 35 dB. At the same time, the investigated DS-AMC-OFDM system can achieve 0.1-1.7 Mbps gains over the conventional adaptive transmission system across the same SNR range. The enhancement of the proposed dynamic sub-channel allocation strategy over the fixed strategy is due mainly to the increase in the transmitted data size according to Eq.

TABLE III  
DYNAMIC NUMBER OF THE PILOT AND DATA SYMBOLS FOR EACH SUB-CHANNEL.

$\vartheta_p(i)$	$\vartheta_d(i)$	$\lambda(i)$	$\Gamma_{var}(i)$	$\gamma_{i,\min}(i)$ dB
48	288	0	otherwise	
28	308	20	$0.5 \geq \Gamma_{var}(i) > 0.3$	$10 \leq \gamma_{i,\min}(i) < 20$
8	328	40	$0.3 \geq \Gamma_{var}(i) > 0.2$	$20 \leq \gamma_{i,\min}(i) < 25$
4	332	44	$0.2 \geq \Gamma_{var}(i) > 0.1$	$25 \leq \gamma_{i,\min}(i) < 30$
2	334	46	$\Gamma_{var}(i) \leq 0.1$	$\gamma_{i,\min}(i) \geq 30$

(31). The pilots number is reduced for the stable sub-channel profiles individually, followed by replacing the unused pilot symbols with additional data symbols based on Eq. (28)-(30). On the other hand, the DS-AMC-OFDM scheme throughput improvement in comparison with the conventional AMC method is achieved by the optimal MCS selection for each sub-channel as explained in the previous section. It is observed from the plots that the pilots number reduction has not influenced the performance of the system significantly.

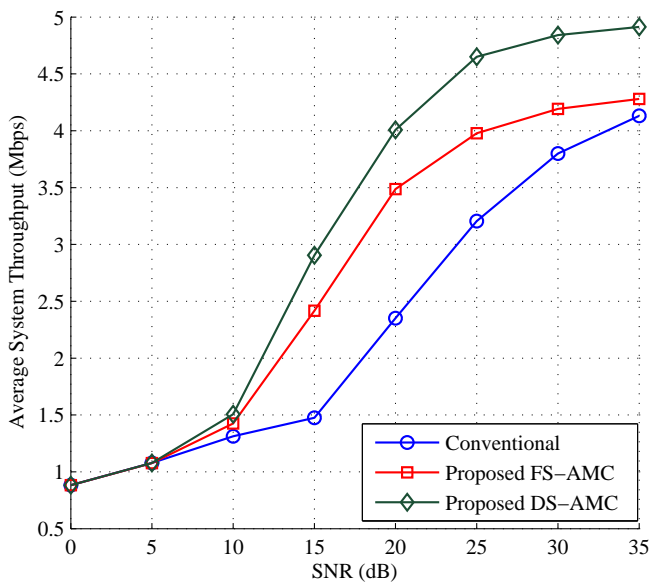


Fig. 12. Throughput of the proposed conventional, FS-AMC-OFDM, and DS-AMC-OFDM systems.

Fig. 13 illustrates the BER performance of the investigated systems. It can be seen that the BER plot for the DS-AMC-OFDM system is approximately converging to the FS-AMC-OFDM scheme. Although there is an increase in the transmitted data size of the DS-AMC-OFDM system, the BER performance is similar to the FS-AMC-OFDM system. It is highlighted that the performance similarity proves that the reduction in pilot size across the sub-channel has not influenced the data recovery, which is based on the channel estimation, at the receiver. Both proposed strategies perform better than the conventional adaptive transmission method, particularly between SNR values of 10 to 25 dB. Meanwhile all compared systems' plots are converging together for high

SNR values due to the similarity of selection the highest MCS for all sub-channels. The BER enhancement of both proposed systems is due to the independent selection of suitable MCS for each sub-channel independently.

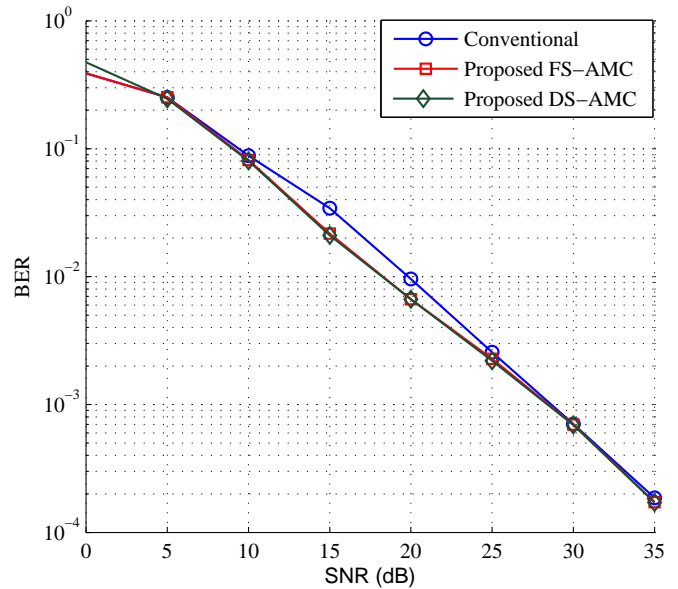


Fig. 13. BER of the conventional, FS-AMC-OFDM, and DS-AMC-OFDM systems.

The comparison of the transmitted data size in bits between the conventional AMC, proposed FS-AMC-OFDM, and proposed DS-AMC-OFDM schemes is presented in Fig. 14. It is observed that the size of the transmitted data for the proposed system based on the dynamic sub-channel allocation strategy is significantly larger by 0.1-0.7 Mbit in comparison with the FS-AMC-OFDM system. Moreover, the DS-AMC-OFDM scheme outperforms the conventional AMC in terms of transmitted data size by 0.1-1.7 Mbit over the SNR range between 5 and 35 dB. The increase in the transmitted data size of the DS-AMC-OFDM system over the other investigated systems is achieved by reducing the number of pilots without affecting the channel estimation performance. Meanwhile, the redundant pilots are replaced by additional data symbols for each sub-channel individually. As mentioned earlier, the reduction in pilot number is restricted by two main metrics; the sub-channel minimum SNR value, and the variance of the sub-channel SNR fluctuation values as expressed in Eq. (30).

In order to monitor the effects of pilot number reduction for each sub-channel independently, the MSE for the estimated channel is evaluated as shown in Fig. 15. The figure shows that the reduction in the number of pilots for the sub-channels with stable profile affects the estimation accuracy after 10 dB. However, the degradation in terms of data recovery errors is acceptable as demonstrated in Fig. 12 in the system throughput performance. The MSE values for both the proposed systems channel estimation is calculated according to Eq. (29).

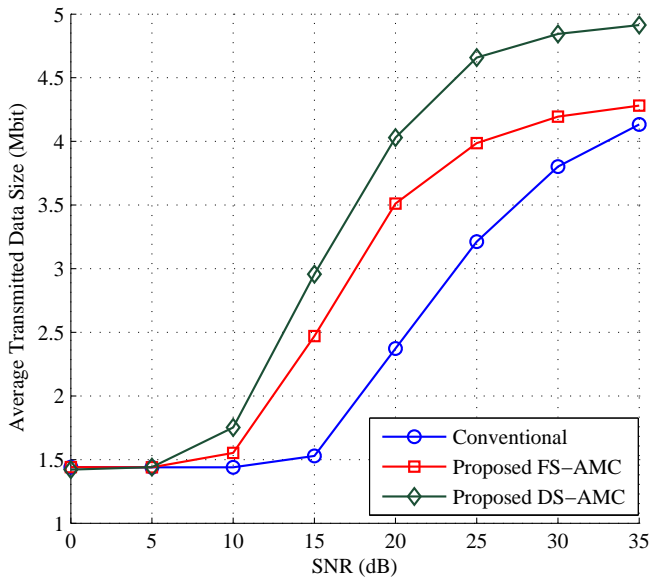


Fig. 14. Transmitted data of the conventional, FS-AMC-OFDM and DS-AMC-OFDM systems.

As a result, the proposed FS-AMC-OFDM and DS-AMC-OFDM systems outperform the conventional approach for different values of SNR. The proposed FS-AMC-OFDM system can perform similar to the conventional scheme over flat fading channels due to the same selection of the MCS level for all sub-channels.

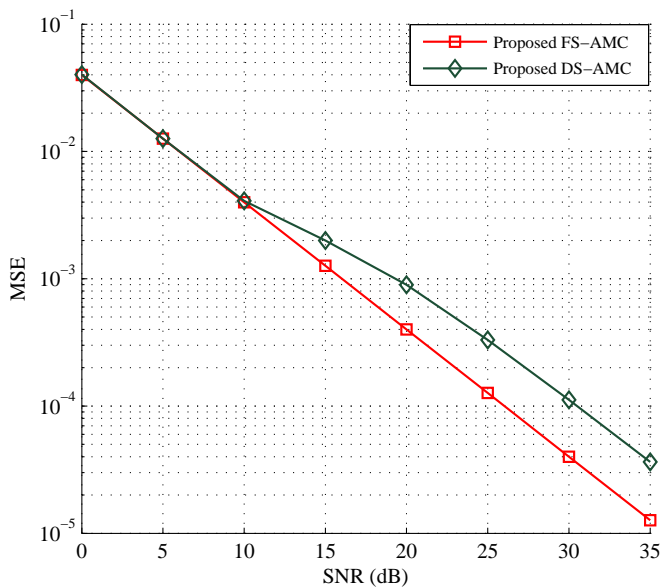


Fig. 15. MSE of the estimated channel for the FS-AMC-OFDM, and DS-AMC-OFDM systems.

## VI. CONCLUSIONS

In this paper, we have proposed FS-AMC-OFDM and DS-AMC-OFDM schemes and their performance has been investigated in Rayleigh fading channels. In order to improve the throughput and BER performance of the proposed FS-AMC-OFDM scheme, the detected coherence bandwidth of the channel has been employed as an important indicator for dividing the OFDM frame into distinct sub-channels and subsequently assigning individual modulation schemes and coding rates suited to the corresponding channel conditions. The throughput is improved in the FS-AMC-OFDM system by exploiting the fading diversity of the channel, which results in increased coding rate and modulation orders, which are utilized for sub-channels with stable fading profiles. Moreover, the optimal MCS selection for each sub-channel increases the aggregate system throughput by decreasing the BER due to the optimal utilization of the channel state for each sub-channel at the transmitter.

On the other hand, the throughput performance of the investigated DS-AMC-OFDM system is improved in comparison with the conventional and FS-AMC-OFDM schemes due to the increase in the transmitted data size, achieved by replacing the redundant pilots with data symbols. The redundant pilots result from the pilot reduction across the stable sub-channel profiles, based on the individual sub-channel minimum SNR value, and the variance of the sub-channel fluctuation values. In order to measure the effects of the pilot reduction on the channel estimation process, the MSE value of the estimated channel was evaluated.

Simulation results have demonstrated that both the system throughput and BER of the DS-AMC-OFDM system are improved compared to the FS-AMC-OFDM scheme and conventional adaptive approach. At the same time, the proposed FS-AMC-OFDM scheme also outperforms the conventional system.

Future work will be focused on enhancing the channel estimation methods to further improve in the BER and throughput performances of the proposed strategies. Moreover, it is worth to investigate the ability of implementing the proposed techniques for long term evolution 3rd generation (LTE-3G) systems and discrete multi-tone modulation (DMT) transmission strategies used in digital subscriber lines (DSL), and the implementation restrictions in terms of the utilized system parameters.

## REFERENCES

- [1] M. Al-Janabi, C. Tsimenidis, B. Sharif and S. Le Goff, "Adaptive MCS Selection in OFDM Systems Based on Channel Frequency Coherence, *AICT 2009*, pp: 177-182.
- [2] D. Tse, *Fundamentals of Wireless Communications*, University of California, Berkeley, 2004.
- [3] R. van Nee and R. Prasad, *OFDM for Wireless Multimedia Communications*, Artech House, 2000.
- [4] A. L. Intini, *Orthogonal Frequency Division Multiplexing for Wireless Networks*, University of California Santa Barbara, 2000.
- [5] H. Schulze and Ch. Luders, *Theory and Applications of OFDM and CDMA Wideband Wireless Communications*, John Wiley and Sons Ltd, Chichester, 2005.
- [6] U. Madhow, *Fundamentals of Digital Communication*, Cambridge University Press, 2004.

- [7] L. Nuaymi, *WiMAX Technology for Broadband Wireless Access*, John Wiley and Sons, Ltd, England, 2007.
- [8] T. Onodera, T. Nogami, O. Nakamura and N. Okamoto, "AMC Design for Wideband OFDM Maintaining Target Quality Over Time-Varying Channels," *IEEE 18th International PIMRC 2007*, pp:1-5.
- [9] R. G. Gallager, *Low-Density Parity-Check Codes*, MIT Press, Cambridge, MA, 1963.
- [10] D. J. C. MacKay, "Good Error-Correction Codes Based on Very Sparse Matrices", *IEEE Trans. on Inform. Theory*, vol. 45, no. 2, pp: 399-431, Mar. 1999.
- [11] M. Zhou, L. Li, N. Wen, et al., "Performance of LDPC coded AOFDM under frequency-selective fading channel," Intern. Conf. on Commun., *ICCCAS 2006*, pp: 861-865.
- [12] L. Lihua, Z. Mingyu, W. Haifeng and Z. Ping, "LDPC coded AMC based on decoding iteration times for OFDM systems," *VTC 2006*, pp: 1157-1161.
- [13] K. Song, A. Ekbal, S. Chung and J. Cioffi, "Adaptive Modulation and Coding (AMC) for Bit-Interleaved Coded OFDM (BICM-OFDM)", *IEEE Trans. on Wireless Commun.*, vol.5, No.7, pp: 1685-1694, Jul. 2006.
- [14] S. Chung, C. Sung, J. Heo and I. Lee, "Adaptive Bit-Interleaved Coded OFDM With Reduced Feedback Information", *IEEE Trans. Commun.*, Vol.55, No.9, pp: 1649-1655, Sep. 2007.
- [15] J. Heo, Y. Wang, and K. Chang, "A Novel Two-Step Channel-Prediction Technique for Supporting Adaptive Transmission in OFDM/FDD System," *IEEE Trans. Veh. Technol.*, Vol. 57, No. 1, pp: 188-193, Jan. 2008.
- [16] T. Kwon and D. Cho, "Adaptive-Modulation-and-Coding-Based Transmission of Control Message for Resource Allocation in Mobile Communication Systems," *IEEE Trans. Veh. Technol.*, Vol. 58, No. 6, pp: 2769-2782, Jul. 2009.
- [17] H. Fu and D. Kim, "Scheduling Performance in Downlink WCDMA Networks with AMC and Fast Cell Selection," *IEEE Trans. Wireless Commun.*, Vol. 7, No. 7, pp: 2580-2591, Jul. 2008.
- [18] H. Yang and S. Sasakan, "Analysis of Channel-Adaptive Packet Transmission Over Fading Channels With Transmit Management," *IEEE Trans. Veh. Technol.*, Vol. 57, No. 1, pp: 404-413, Jan. 2008.
- [19] R. Kwan and C. Leung, "Performance of a CDMA System Employing AMC and Multicodes in the Presence of Channel Estimation Errors," *IEEE Trans. Commun.*, Vol. 56, No. 2, pp: 189-193, Feb. 2008.
- [20] P. Tan, Y. Wu and S. Sun, "Link Adaptation Based on Adaptive Modulation and Coding for Multiple-Antenna OFDM System," *IEEE J. in Select. Area Commun.*, Vol. 26, No. 8, pp: 1599-1606, Jul. 2008.
- [21] K. Ishihara, Y. Takatori, S. Kubota and M. Umehira, "Comparison of SCFDE and OFDM with adaptive modulation and coding in nonlinear fading channel," *Electronic Letters*, Vol. 43, No. 3, pp: 174-175, Feb. 2007.
- [22] L. Caponi, F. Chiti and R. Fantacci, "Performance Evaluation of a Link Adaptation Technique for High Speed Wireless Communication Systems," *IEEE Trans. Wireless Commun.*, Vol. 6, No. 12, pp: 4568-4575, Dec. 2007.
- [23] X. Wang, Q. Liu and G. Giannakis, "Analyzing and Optimizing Adaptive Modulation Coding Jointly With ARQ for QoS-Guaranteed Traffic," *IEEE Trans. Wireless Commun.*, Vol. 7, No. 7, pp: 1008-1013, Jul. 2008.
- [24] L. Ye, A. Burr, "Adaptive modulation and code rate for turbo coded OFDM transmissions," *VTC 2007*, pp: 2702-2706.
- [25] N. Miki, Y. Kishiyama, M. Sawahashi, "Optimum Adaptive Modulation and Coding Scheme for Frequency Domain Channel-Dependent Scheduling in OFDM Based Evolved UTRA Downlink," *IEEE WCNC 2007*, pp: 1783-1788.
- [26] N. Benvenuto and F. Tosato, "On the Selection of Adaptive Modulation and Coding Modes over OFDM," *Communications, IEEE ICC 2004*, pp: 3251-3255.
- [27] T. Moon, *Error Correction Coding, Mathematical Methods and Algorithms*, John Wiley and sons, INC., Canada, 2005.
- [28] C. Lim and D. Han, "Robust LS Channel Estimation with Phase Rotation for Single Frequency Network in OFDM," *IEEE Transactions on Consumer Electronics* Vol. 52, No. 4, pp: 1173-1178, Nov. 2006.



[www.iariajournals.org](http://www.iariajournals.org)

**International Journal On Advances in Intelligent Systems**

✦ ICAS, ACHI, ICCGI, UBICOMM, ADVCOMP, CENTRIC, GEOProcessing, SEMAPRO, BIOSYSCOM, BIOINFO, BIOTECHNO, FUTURE COMPUTING, SERVICE COMPUTATION, COGNITIVE, ADAPTIVE, CONTENT, PATTERNS

✦ issn: 1942-2679

**International Journal On Advances in Internet Technology**

✦ ICDS, ICIW, CTRQ, UBICOMM, ICSNC, AFIN, INTERNET, AP2PS, EMERGING

✦ issn: 1942-2652

**International Journal On Advances in Life Sciences**

✦ eTELEMED, eKNOW, eL&mL, BIODIV, BIOENVIRONMENT, BIOGREEN, BIOSYSCOM, BIOINFO, BIOTECHNO

✦ issn: 1942-2660

**International Journal On Advances in Networks and Services**

✦ ICN, ICNS, ICIW, ICWMC, SENSORCOMM, MESH, CENTRIC, MMEDIA, SERVICE COMPUTATION

✦ issn: 1942-2644

**International Journal On Advances in Security**

✦ ICQNM, SECURWARE, MESH, DEPEND, INTERNET, CYBERLAWS

✦ issn: 1942-2636

**International Journal On Advances in Software**

✦ ICSEA, ICCGI, ADVCOMP, GEOProcessing, DBKDA, INTENSIVE, VALID, SIMUL, FUTURE COMPUTING, SERVICE COMPUTATION, COGNITIVE, ADAPTIVE, CONTENT, PATTERNS

✦ issn: 1942-2628

**International Journal On Advances in Systems and Measurements**

✦ ICQNM, ICONS, ICIMP, SENSORCOMM, CENICS, VALID, SIMUL

✦ issn: 1942-261x

**International Journal On Advances in Telecommunications**

✦ AICT, ICDT, ICWMC, ICSNC, CTRQ, SPACOMM, MMEDIA

✦ issn: 1942-2601